Characteristics of aquatic biospheres on temperate planets around Sun-like stars and M dwarfs

Manasvi Lingam[1,2]* and Abraham Loeb[2]

[1]*Department of Aerospace, Physics and Space Sciences, Florida Institute of Technology, Melbourne, FL 32901, USA*
[2]*Institute for Theory and Computation, Harvard University, Cambridge, MA 02138, USA*

ABSTRACT

Aquatic biospheres reliant on oxygenic photosynthesis are expected to play an important role on Earth-like planets endowed with large-scale oceans insofar as carbon fixation (i.e. biosynthesis of organic compounds) is concerned. We investigate the properties of aquatic biospheres comprising Earth-like biota for habitable rocky planets orbiting Sun-like stars and late-type M dwarfs such as TRAPPIST-1. In particular, we estimate how these characteristics evolve with the available flux of photosynthetically active radiation (PAR) and the ambient ocean temperature (T_W), the latter of which constitutes a key environmental variable. We show that many salient properties, such as the depth of the photosynthesis zone and the net primary productivity (i.e. the effective rate of carbon fixation), are sensitive to PAR flux and T_W and decline substantially when the former is decreased or the latter is increased. We conclude by exploring the implications of our analysis for exoplanets around Sun-like stars and M dwarfs.

Key words: astrobiology – planets and satellites: detection – planets and satellites: surfaces – stars: low-mass.

1 INTRODUCTION

It is a well-known fact that the Earth's environment – its lithosphere, hydrosphere, atmosphere, and biosphere – has transformed greatly over time (Lunine 2013; Knoll 2015; Knoll & Nowak 2017; Stüeken et al. 2020), and the same also applies to other terrestrial planets in our Solar system (Ehlmann et al. 2016; Kane et al. 2019). In tandem, there is growing awareness and acceptance of the fact that habitability is a multifaceted and dynamic concept that depends on a number of variables aside from the existence of liquid water (Dole 1964; Kasting 2012; Cockell et al. 2016; Shields, Ballard & Johnson 2016; Cockell 2020; Lingam & Loeb 2021); the latter criterion has been widely employed to demarcate the limits of the so-called habitable zone and its manifold extensions (Huang 1959; Dole 1964; Kasting, Whitmire & Reynolds 1993; Kopparapu et al. 2013, 2014; Ramirez 2018; Ramirez et al. 2019; Schwieterman et al. 2019).

One of the most crucial environmental parameters that regulates myriad biological processes, and thus the propensity for planetary habitability, is the ambient temperature (Cossins & Bowler 1987; Hochachka & Somero 2002; Angilletta 2009; Clarke 2017). It is not surprising, therefore, that there exists a large corpus of work on the thermal limits of life based on comprehensive experiments on thermophiles (Rothschild & Mancinelli 2001; McKay 2014; Clarke 2014; Merino et al. 2019). In recent times, numerical models have employed the thermal limits for Earth-like complex life to assess the habitability of exoplanets for such organisms (Silva et al. 2017; Murante et al. 2020), and similar analyses have been undertaken for generic subsurface biospheres as well (McMahon, O'Malley-James & Parnell 2013; Lingam & Loeb 2020c).

Motivated by these facts, we will study how temperature impacts the prospects for aquatic photosynthesis on Earth-analogues around stars of two noteworthy spectral types. By Earth-analogues, we refer hereafter to rocky planets that are sufficiently similar to Earth in so far as *all* their geological, physical, and chemical properties are concerned. Our reasons for choosing to investigate aquatic photosynthesis are twofold. First, the importance of photosynthesis is well-established from the standpoint of physics and biochemistry as stellar radiation is the most plentiful source of thermodynamic disequilibrium (Deamer & Weber 2010), and photosynthesis represents the dominant avenue for the biosynthesis on organic compounds on Earth (Bar-On; Phillips & Milo 2018).

In particular, we will focus on oxygenic photosynthesis because its electron donor (water) is available in plentiful supply, consequently ensuring that this mechanism is not stymied by the access to electron donors (Ward, Rasmussen & Fischer 2019). Moreover, the advent of oxygenic photosynthesis is known to have profoundly altered Earth's geochemistry and biology (Lane 2002; Judson 2017). We will adopt the conventional range of $\lambda_{min} = 400$ and $\lambda_{max} = 700$ nm for oxygenic photosynthesis (chapter 1.2 in Blankenship 2014), known as photosynthetically active radiation (PAR). To be precise, oxygenic photosynthesis can operate at wavelengths of 350–750 nm (Chen & Blankenship 2011; Nürnberg et al. 2018; Claudi et al. 2021), but the canonical choice of the PAR range delineated above does not alter our subsequent results significantly.

We will not delve into the feasibility of multiphoton schemes that might elevate λ_{max} to longer wavelengths because their efficacy has not been adequately established. On the one hand, it is plausible that the upper bound (namely λ_{max}) for PAR could be boosted to wavelengths of $\gtrsim 1000$ nm (Wolstencroft & Raven 2002; Tinetti, Rashby & Yung 2006; Kiang et al. 2007; Lingam & Loeb 2019e; Lingam, Ginsburg & Loeb 2020). However, on the other hand, these

* E-mail: mlingam@fit.edu

multiphoton schemes may be more fragile and susceptible to low efficiencies due to side reactions (Kiang et al. 2007; Kume 2019; Lingam & Loeb 2020a). Moreover, recent numerical modelling based on empirical data indicates that, while photosynthesis in the near-infrared is feasible, oxygenic photosynthesis on M dwarfs may eventually revert to the conventional PAR range described in the preceding paragraph (Gale & Wandel 2017; Takizawa et al. 2017).

The second reason why we opt to investigate the prospects for aquatic photosynthesis stems from the basic datum that the oceans contribute nearly half to the overall NPP of modern Earth (Field et al. 1998). In fact, Earth was almost exclusively composed of oceans (i.e. virtually devoid of large landmasses) for a certain fraction of its history (Iizuka et al. 2010; Arndt & Nisbet 2012), implying that aquatic photosynthesis may have played an even more significant role in those periods. A few theoretical models have even proposed that continents only emerged in late-Archean era in the neighborhood of 2.5 Gya (Flament, Coltice & Rey 2008; Lingam & Loeb 2021); this conjecture seems to be compatible with the recent analysis of oxygen-18 isotope data from the Pilbara Craton of Western Australia (Johnson & Wing 2020).

Looking beyond Earth, statistical analyses of exoplanets indicate that a substantial fraction of super-Earths are rich in volatiles (Rogers 2015; Wolfgang & Lopez 2015; Chen & Kipping 2017; Zeng et al. 2018; Jin & Mordasini 2018). In particular, some of the Earth-sized planets in the famous TRAPPIST-1 system (Gillon et al. 2017) may fall under this category, with the water fraction potentially reaching values as high as ∼ 10 per cent by mass (Grimm et al. 2018; Unterborn, Hinkel & Desch 2018; Dorn et al. 2018). The habitability of ocean planets (also called water worlds), which are wholly devoid of continents (Kuchner 2003; Léger et al. 2004), has been analysed from multiple standpoints (Abbot, Cowan & Ciesla 2012; Kaltenegger, Sasselov & Rugheimer 2013; Cowan & Abbot 2014; Goldblatt 2015; Noack, Snellen & Rauer 2017; Kite & Ford 2018; Ramirez & Levi 2018; Lingam & Loeb 2019c). In recent times, increasing attention is being directed toward oceanographic phenomena such as salinity, circulation patterns and nutrient up-welling (Hu & Yang 2014; Cullum & Stevens 2016; Lingam & Loeb 2018a; Yang et al. 2019; Checlair et al. 2019; Del Genio et al. 2019; Olson, Jansen & Abbot 2020; Salazar et al. 2020) on such worlds. However, a detailed treatment of the salient characteristics of aquatic photosynthesis remains missing for the most part.

It is important to recognize that we will deal with aquatic environments, but this does not necessarily imply that all worlds under consideration must be solely composed of oceans. The outline of this paper is as follows. We commence with a description of some of the basic tools needed to facilitate our analysis in Section 2. We proceed thereafter by calculating how the properties of aquatic photosynthesis such as the compensation depth and the net primary productivity (NPP) vary with the PAR flux and ocean temperature in Section 3. Next, we explain the salient model limitations in Section 4. Subsequently, we delineate the ramifications arising from our modelling for Earth-like exoplanets in Section 5, and we conclude with a synopsis of our central findings in Section 6.

2 MATHEMATICAL PRELIMINARIES

In order to study the basic characteristics of aquatic photosynthesis and their dependence on the average ocean temperature (T_W), we hold all parameters (biological, geological, and astrophysical) identical to that of Earth. We consider two different Earth-analogues hereafter: one around a solar twin (Planet G) and the other around a late-type M dwarf (Planet M) with effective temperatures of $T_\odot = 5780$ and $T = 2500$ K, respectively. Planet M is taken to be *tidally locked* (Barnes 2017), and the star that it orbits has a temperature closely resembling that of TRAPPIST-1 (Delrez et al. 2018). The reason for doing so is that Sun-like stars are considered 'safe' targets for biosignature searches (Kasting et al. 1993; Heller & Armstrong 2014; Lingam & Loeb 2018c), whereas the habitability of M-dwarf exoplanets, especially those orbiting active stars, remains subject to many ambiguities (Tarter et al. 2007; Scalo et al. 2007; Shields et al. 2016; Lingam & Loeb 2019b).

In what follows, we draw upon two major simplifying assumptions. First, we model the star as an idealized blackbody with an effective temperature of T. Secondly, we account for the attenuation of PAR after the passage through the atmosphere by introducing a fudge factor. While neither of these simplifications are entirely realistic, the global results are known to deviate from more realistic models and data by a factor of only less than 1.5 for the most part (Lingam & Loeb 2020b).[1] The reason for this reasonable degree of accuracy stems from the fact that most of the basic quantities we compute hereafter exhibit a weak (i.e. semi-logarithmic) dependence on the two assumptions outlined above.

As we are dealing with Earth-analogues, the stellar flux at the planet's location is taken to be $S_\oplus \approx 1360$ W m^{-2}. At the substellar point on the planet, the photon flux density ($\mathcal{N}_{\max}$) at the top of the atmosphere is given by

$$\mathcal{N}_{\max}(\lambda) \approx n_\lambda \left(\frac{R_\star}{d_\star}\right)^2, \tag{1}$$

with $R_\star$ and $d_\star$ constituting the stellar and orbital radius, respectively, whereas n_λ is the photon flux density of the star at its surface. The blackbody brightness B_λ is invoked to yield

$$n_\lambda = \frac{B_\lambda}{(hc/\lambda)} = \frac{2c}{\lambda^4} \left[\exp\left(\frac{hc}{\lambda k_B T}\right) - 1\right]^{-1}, \tag{2}$$

where λ is the photon wavelength. As we have assumed the stellar flux is equal to $S_\oplus$ for the Earth-analogues, we can express $d_\star$ as follows:

$$d_\star = \sqrt{\frac{L_\star}{4\pi S_\oplus}}, \tag{3}$$

where the stellar luminosity ($L_\star$) is given by $L_\star = 4\pi\sigma R_\star^2 T^4$. After employing this relation in (1), we find that $\mathcal{N}_{\max}$ transforms into

$$\mathcal{N}_{\max}(\lambda) \approx \frac{n_\lambda S_\oplus}{\sigma T^4}. \tag{4}$$

It is, however, necessary to recognize that $\mathcal{N}_{\max}$ constitutes an upper bound for the photon flux density at the surface for two reasons. First, this photon flux density is calculated at the zenith, and therefore ignores the fact that a given location will not always correspond to the substellar point. Secondly, the effects of clouds and atmospheric attenuation are neglected. Hence, a more viable expression for the photon flux density at the planet's surface ($\mathcal{N}_{\text{avg}}$) is given by

$$\mathcal{N}_{\text{avg}}(\lambda) \approx \mathcal{N}_{\max}(\lambda) \times f_I \times f_{CL}, \tag{5}$$

with f_{CL} embodying the total atmospheric attenuation (chapter 4.2 in Sarmiento & Gruber 2006), and f_I quantifying the average intensity of

---

[1] In fact, the spatial heterogeneity inherent to oceans are known to introduce local variations that are more than an order of magnitude greater than this factor (Behrenfeld et al. 2005), owing to which the estimates in Lingam & Loeb (2020b) can be regarded as fairly accurate global values.

light at a given location as a fraction of the intensity at the substellar point. Henceforth, we adopt $f_A \equiv f_I \times f_{CL} \approx 0.2$ for reasons elucidated further in Lingam & Loeb (2020b) and to maintain compatibility with Earth's global parameters (chapter 4.3 in Sarmiento & Gruber 2006); altering this fraction by a factor of order unity does not change our results significantly due to the logarithmic dependence alluded to earlier in this section. With this choice of f_A, it should be noted that $\mathcal{N}_{avg}(\lambda) \approx 0.2 \mathcal{N}_{max}(\lambda)$.

Although the above choice has been motivated in Lingam & Loeb (2020b), a recapitulation is warranted at this stage. On the one hand, f_I is higher for M-dwarf exoplanets due to the fact that the tidally locked dayside does not experience nights and is bathed in continual illumination (Gale & Wandel 2017). On the other hand, f_{CL} is reduced as a consequence of the potentially higher atmospheric absorptivity and increased cloud clover, among other factors (Kasting et al. 1993; Yang, Cowan & Abbot 2013; Kopparapu et al. 2016). Therefore, by specifying f_A to be constant (as we did in the previous paragraph), we are effectively already ensuring that the atmospheric attenuation experienced by M-dwarf Earth-analogues is a few times higher than their counterparts around Sun-like stars, in line with prior theoretical predictions.

We have verified that quantities such as the compensation depth, the critical depth, and the net primary productivity (all of which are defined later) decrease by a factor of $\lesssim 2$, *ceteris paribus*, even up to nearly an order of magnitude increase in the degree of atmospheric attenuation. Lastly, we remark that the interplay of all the aforementioned variables is further complicated by the presence of climate feedback mechanisms as well as the atmospheric and surface compositions that may collectively yield different values from one climate model to another, even for the same setup, which makes estimating them challenging (Zsom et al. 2013; Shields et al. 2016; Cullum & Stevens 2016). Assessing the properties of aquatic photosynthesis is a complicated task, as elucidated in Section 4, owing to which our goal herein is to primarily focus on understanding how the salient characteristics vary as a function of key *physical* parameters that can be constrained by present-day or forthcoming observations (Fujii et al. 2018).

Given the photon flux density, denoted by $\mathcal{N}_0(\lambda)$, at the surface, we are in a position to calculate the photon flux $\mathcal{F}$ at a depth z below the surface of the ocean. This quantity is found by convolving $\mathcal{N}_0(\lambda)$ and the vertical attenuation coefficient K in the oceans, thus yielding

$$\mathcal{F}(z) \approx \int_{\lambda_{min}}^{\lambda_{max}} \mathcal{N}_0(\lambda) \exp(-Kz) \, d\lambda. \qquad (6)$$

It should be noted that $\mathcal{N}_0(\lambda)$ is equal to $\mathcal{N}_{max}$ or $\mathcal{N}_{avg}$, depending on what scenario we wish to analyse. Now, let us turn our attention to K, which we shall rewrite as $K = K_W + K_I$ (chapter 9.5 in Kirk 2011). The first term (K_W) is the attenuation coefficient associated with water whereas K_I accounts for the attenuation stemming from impurities as well as biota. In order to tackle K_W, we begin by noting that it has been tabulated as a function of λ in many sources (Hale & Querry 1973; Smith & Baker 1981; Kou, Labrie & Chylek 1993; Litjens, Quickenden & Freeman 1999; Morel et al. 2007). Based on the data taken from Pope & Fry (1997, table 3), which are consistent with later studies over the PAR range (Lee et al. 2015), the following simple exponential fit was employed by Lingam & Loeb (2020b) across the PAR range:

$$K_{W,22} \approx 1.4 \times 10^{-5} \, \text{m}^{-1} \exp\left(\lambda \times 1.54 \times 10^7 \, \text{m}^{-1}\right), \qquad (7)$$

although it is essential to recognize that the data had been collected at 22°C (table 3 in Pope & Fry 1997). In general, K_W is not only dependent on λ but also on T_W. The ocean temperature in turn varies with depth, but it only changes by a few K in the zone where the bulk of photosynthesis occurs (Pawlowicz 2013). Hence, we shall treat T_W as being roughly constant, thereby enabling us to model it as a free parameter in the model. In order to account for the dependence on T_W, we employ the linear temperature scaling that has been confirmed by a number of empirical studies (Langford, McKinley & Quickenden 2001; Sullivan et al. 2006; Röttgers, McKee & Utschig 2014), thereupon enabling us to write

$$K_W(T_W, \lambda) = K_{W,22} + \alpha(\lambda)\Delta T_{22}, \qquad (8)$$

where $\alpha(\lambda)$ represents the wavelength-dependent temperature coefficient (units of $\text{m}^{-1} \, \text{K}^{-1}$), and $\Delta T_{22} = T_W - 295$ is a measure of the deviation from the standard water temperature of 22°C employed in calculating $K_{W,22}$.

For the PAR range considered herein, the second term on the right-hand side of the above expression is always much smaller than the first term provided that ΔT_{22} is $\mathcal{O}(10)$ K. This condition arises because α is nearly zero across the PAR range ($\lesssim 10^{-3} \, \text{m}^{-1} \, \text{K}^{-1}$), as can be verified by comparing Röttgers et al. (2014, fig. 5) and Sullivan et al. (2006, table 1) with Pope & Fry (1997, table 3). Apart from the temperature dependence, we remark that K_W also exhibits a dependence on the salinity, which is naturally expected to vary from one ocean to another (Cullum & Stevens 2016; Olson et al. 2020). However, we have implicitly held the salinity fixed to that of the global value of Earth's oceans. More importantly, the salinity dependence is weak across the PAR range, as shown by experimental studies (Sullivan et al. 2006; Röttgers et al. 2014).

Next, we turn our attention to the other attenuation coefficient K_I. If one considers the case with pure water, i.e. amounting to $K_I \to 0$, it follows that $\mathcal{F}$ is maximized for a given depth *ceteris paribus*. In a more realistic setting, however, we shall adopt $K_I \approx 0.08 \, \text{m}^{-1}$ to maintain consistency with the typical diffuse attenuation coefficient in the PAR range for Earth's oceans (chapter 4.2 in Sarmiento & Gruber 2006); this choice is also compatible with the coefficients deduced from measurements of clear ocean waters (Lee et al. 2005; Saulquin et al. 2013; Son & Wang 2015). In actuality, K_I will also be a function of wavelength and temperature, but the exact dependence is dictated by several complex oceanographic and biological (e.g. density of photoautotrophs) factors (Morel et al. 2007), owing to which we have opted to work with a constant value. The wavelength variation, in particular, is rather weak because K_I changes by only a factor of ~ 2 across the PAR range (fig. 4 in Morel & Maritorena 2001).

At this stage, it is worth recapitulating the two broad scenarios we shall be considering. The first corresponds to the so-called idealized case where the star is located at the substellar point, and there is no attenuation because of the atmosphere and oceanic impurities. In other words, we employ $\mathcal{N}_0(\lambda) = \mathcal{N}_{max}$ and $K = K_W$, and introduce the superscript 'I' (for idealized). This outcome was studied extensively by Ritchie, Larkum & Ribas (2018), albeit with an exclusive focus on Earth and Proxima b. The second case accounts for time-averaged stellar flux and the existence of biological attenuation. Here, we select $\mathcal{N}_0(\lambda) = \mathcal{N}_{avg}$, $K = K_W + K_I$ and the non-zero value of K_I defined in the prior paragraph, and label it using the superscript 'A', to wit, the 'global average' case. For each of these two scenarios, we consider two different Earth-analogues (Planets G and M) delineated at the beginning of this section. For Planet M, however, the 'global average' refers to the *dayside* parameters, e.g. the variable T_W represents the average temperature on the dayside of the tidally locked M-dwarf exoplanet.

3 CHARACTERISTICS OF AQUATIC BIOSPHERES

In this section, we examine how certain the salient properties of aquatic biospheres depend on the ocean temperature; in some cases, we investigate the joint dependence on stellar and ocean temperatures. Before embarking on the discussion, we will define the quantities of interest that appear herein; for a historical treatment, we defer to Mills (2012) and Behrenfeld & Boss (2018).

The first concept that we introduce from biological oceanography is the euphotic zone depth: the location where the photon flux becomes 1 per cent of its surface value. As one can see from the definition, it is divorced from biological properties for the most part. The euphotic zone depth is commonly interpreted as a measure of the photosynthesis zone on Earth, but it does not constitute a reliable metric in actuality (Banse 2004; Marra et al. 2014). Before proceeding ahead, we note that the depth of the euphotic zone decreases from ∼10 to 100 m for Earth-analogues orbiting Sun-like stars to $\mathcal{O}(1)$ m for tidally locked late-type M-dwarf exoplanets (Ritchie et al. 2018; Kaltenegger 2019; Lingam & Loeb 2020b).

Next, we consider the compensation depth ($\mathcal{Z}_{CO}$), which is determined by calculating the location at which $\mathcal{F}(z)$ is equal to the compensation flux ($\mathcal{F}_C$). The latter is roughly defined as the flux at which the rate of growth via photosynthesis becomes equal to the rate of respiration (Gaarder & Gran 1927; Marshall & Orr 1928); in other words, at this depth, the net growth rate of the photoautotroph under consideration is equal to zero at $\mathcal{Z}_{CO}$. As per the definition, the compensation depth is regulated by $\mathcal{F}(z)$, which, in turn, *inter alia*, depends on the parameter f_I introduced in Section 2. Here, it is important to appreciate that f_I is *different* for M- and G-type exoplanets (Lingam & Loeb 2020b), due to the fact the dayside of the former receives permanent illumination when tidally locked (amounting to higher f_I broadly speaking). Although f_I functions as a fudge factor to an extent, we acknowledge that it does not fully capture the distinct spatiotemporal differences in light distribution, or oceanic properties like nutrient upwelling (Lingam & Loeb 2018a; Olson et al. 2020), associated with tidally locked M-dwarf exoplanets.

The other quantity of interest is the critical depth ($\mathcal{Z}_{CR}$), which was elucidated by Gran & Braarud (1935) and placed on a quantitative footing by Riley (1946) and Sverdrup (1953). It can be envisioned as the integrated (i.e. global) version of the compensation depth. The critical depth is the location where the *vertically integrated* net growth rate becomes zero, i.e. the integrated photosynthetic growth rate is equal to the integrated depletion rate arising from respiration and other factors (chapter 3 in Mann & Lazier 2006). The critical depth is relevant from an observational standpoint because it may regulate the feasibility of phytoplankton blooms (Falkowski & Raven 2007), which have been posited as an example of temporal biosignatures (Lingam & Loeb 2018a; Schwieterman et al. 2018). If the ocean mixed layer depth is greater than the critical layer depth,[2] the initiation of phytoplankton blooms is rendered unlikely, and vice-versa (pg. 94 of Mann & Lazier 2006). Although the critical depth concept remains influential and useful to this day (Nelson & Smith 1991; Obata, Ishizaka & Endoh 1996; Siegel, Doney & Yoder 2002; Chiswell 2011; Kirk 2011; Fischer et al. 2014; Sathyendranath,

Ji & Browman 2015), it has been subjected to some criticism (Smetacek & Passow 1990; Behrenfeld 2010; Behrenfeld & Boss 2018).

Thus, broadly speaking, the compensation depth and the critical depth represent important concepts inasmuch as exo-oceanography is concerned because they enable us to gauge the depths at which photosynthetic organisms can exist and/or give rise to tangible biosignatures (Sverdrup, Johnson & Fleming 1942; Sverdrup 1953). We refer to Falkowski & Raven (2007, fig. 9.5) for a schematic overview of these two quantities along with the euphotic zone depth.

3.1 Compensation depth

The key point worth appreciating when it comes to the compensation depth is that the compensation flux ($\mathcal{F}_C$) is *not* constant even for a given organism because it is intrinsically temperature-dependent. Thus, our chief objective is to find a suitable function that will adequately describe the behaviour of $\mathcal{F}_C$ with respect to T_W.

In the classical model for the compensation flux, it is proportional to Γ_R/Γ_P – see Riley (1946), Sverdrup (1953), Siegel et al. (2002, equation 2), and Mann & Lazier (2006, chapter 3) – where Γ_R and Γ_P signify the rates of respiration and photosynthesis, respectively. Thus, if we know how these rates vary with temperature, one can duly formulate the expression for $\mathcal{F}_C$. The temperature dependence of these rates is subject to uncertainty and many different fitting functions have been considered. However, both the well-known metabolic theory of ecology (Gillooly et al. 2001; Brown et al. 2004; Dell, Pawar & Savage 2011; Bruno, Carr & O'Connor 2015; Clarke 2017) and recent analyses of empirical data from Earth's oceans (fig. 3.3 in Kirchman 2018) predict that these rates are fairly well described by the classic Arrhenius equation.

Hence, by utilizing the respective activation energies for these two processes (section 3 in Regaudie-De-Gioux & Duarte 2012), we end up with

$$\frac{\Gamma_R}{\Gamma_P} \propto \exp\left(-\frac{\Delta E}{k_B T_W}\right), \tag{9}$$

where $\Delta E \approx 0.34$ eV constitutes the 'net' activation energy, i.e. the difference between the corresponding activation energies (Yvon-Durocher et al. 2012). An important point worth noting is that the above ansatz for Γ_R/Γ_P is monotonically increasing with temperature. It is very unlikely that this behaviour would be obeyed *ad infinitum* because the Arrhenius equation breaks down beyond a certain temperature (Kingsolver 2009; Angilletta 2009; Schulte 2015). The issue, however, is that the optimum temperature, after which the trend reverses, is species-dependent (Clarke 2017; Corkrey et al. 2018), and is modulated to a substantial degree by the environment(s) of the putative organisms. We will restrict ourselves to $273 < T_W < 323$ K, as this interval roughly overlaps with the temperature range of $280 < T_W < 322$ K studied in Barton et al. (2020, pg. 724). In that study, diverse marine phytoplankton were shown to obey (9) for a broad thermal range.

By utilizing the above relationships, the temperature dependence of $\mathcal{F}_C$ is modelled as

$$\mathcal{F}_C \approx 10 \, \mu\text{mol m}^{-2} \, \text{s}^{-1} \, \mathcal{G}(T_W), \tag{10}$$

where we have introduced the auxiliary function,

$$\mathcal{G}(T_W) \equiv \exp\left[13.6\left(1 - \frac{T_0}{T_W}\right)\right], \tag{11}$$

---

[2]As the name indicates, the mixed layer refers to the region of the ocean that is characterized by nearly uniform characteristics (e.g. temperature and salinity), and is governed by the vertical potential density gradient (Kirk 2011; Middelburg 2019).
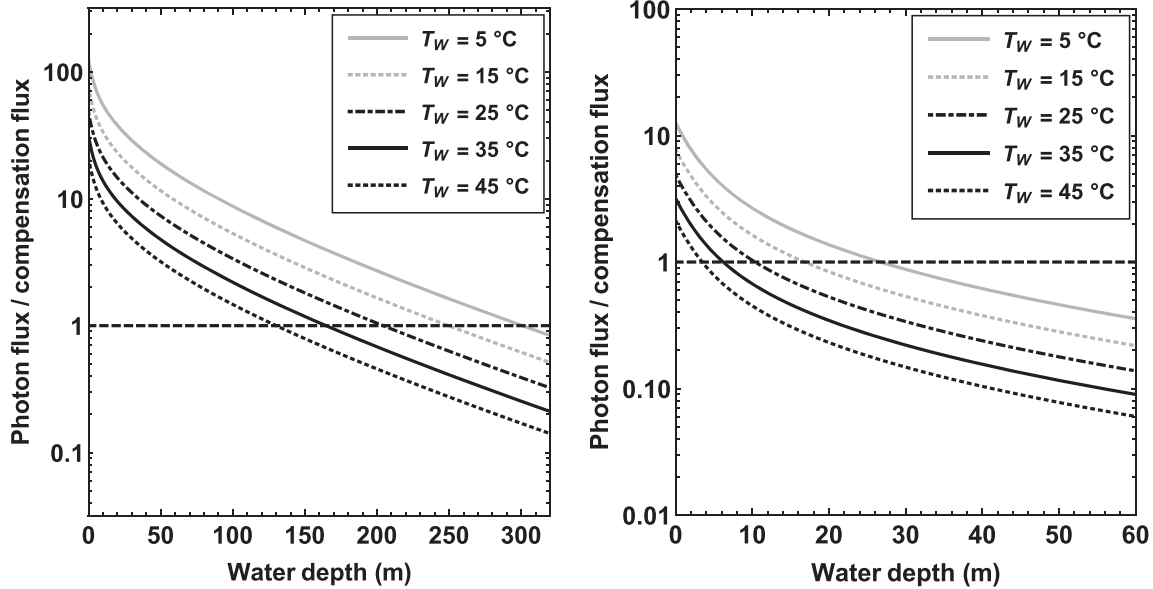
Figure 1. In both panels, the photon flux in units of the compensation flux is shown as a function of the ocean depth for the idealized case described in Section 2; the compensation flux specifies the photon flux below which the net growth of the organism is not feasible. The various curves correspond to different choices of the global ocean temperature, and the intersection points of the various curves with the dashed horizontal line yield the compensation depths. The left- and right-hand panels correspond to Planets G and M, respectively, introduced in Section 2.

with $T_0 \approx 289$ K representing the global surface temperature of Earth's oceans.[3] The constant of proportionality in (10) has been chosen as it represents the compensation flux for phytoplankton in Earth's oceans within a factor of ~ 2 (Nelson & Smith 1991; Marra 2004; Mann & Lazier 2006; Regaudie-De-Gioux & Duarte 2010). By solving for $\mathcal{F}(z) = \mathcal{F}_C$, we are now equipped to calculate the compensation depth $\mathcal{Z}_{CO}$ as a function of both the stellar temperature and ocean temperature.

In Fig. 1, the photon flux normalized by the compensation flux is plotted as a function of the depth z for the idealized case delineated in Section 2, where the star is at the substellar point and the attenuation in water is assumed to be minimal. The left-hand panel corresponds to Planet G, while the right-hand panel depicts the results for Planet M. By inspecting both panels, we find that $\mathcal{Z}_{CO}$ decreases with the temperature along expected lines. The physical reason for this trend is that the increase in the rate of respiration outpaces that of photosynthesis when the temperature is elevated, thereby ensuring that the location at which the two processes balance each other is shifted closer to the surface of the ocean, i.e. leading to a reduction in $\mathcal{Z}_{CO}$.

We observe that the ocean temperature exerts a fairly significant effect on the magnitude of $\mathcal{Z}_{CO}$ for both worlds. As far as Planet G (orbiting a solar twin) is concerned, the compensation depth changes from $\mathcal{Z}_{CO}^{(I)} \approx 300$ m at $T_W = 5°$C to $\mathcal{Z}_{CO}^{(I)} \approx 130$ m at $T_W = 45°$C. On the other hand, when we consider Planet M, situated around a late-type M dwarf closely resembling TRAPPIST-1, the compensation depth morphs from $\mathcal{Z}_{CO}^{(I)} \approx 26.5$ m at $T_W = 5°$C to $\mathcal{Z}_{CO}^{(I)} \approx 3.5$ m at $T_W = 45°$C. Hence, for the idealized case studied in this figure, we predict that the ocean temperature might cause $\mathcal{Z}_{CO}$ to change by nearly an order of magnitude for Planet M; the variation associated with Planet G is smaller, but still non-negligible.

Fig. 2 is analogous to that of Fig. 1, except that we consider the so-called global average case described at the end of Section 2 in lieu of the idealized scenario. When it comes to Planet G (left-hand panel), the compensation depth evolves from $\mathcal{Z}_{CO}^{(A)} \approx 24$ m at $T_W = 5°$C to $\mathcal{Z}_{CO}^{(A)} \approx 8.5$ m at $T_W = 45°$C. However, a striking result is manifested vis-à-vis Planet M (right-hand panel). At $T_W = 5°$C, we obtain $\mathcal{Z}_{CO}^{(A)} \approx 3$ m, but we end up with $\mathcal{Z}_{CO}^{(A)} = 0$ at $T_W = 45°$C. The null value arises because the temperature elevates the compensation point to such an extent that it overshoots the incident photon flux at the ocean's surface.[4] In fact, we determine that $\mathcal{F}_0 \equiv \mathcal{F}^{(A)}(z = 0) < \mathcal{F}_C$ is fulfilled when $T_W > 24°$C, implying that ocean temperatures above this value appear to be relatively unsuitable for supporting phytoplankton-like biota on tidally locked Earth-analogues orbiting stars akin to TRAPPIST-1.

Motivated by the above finding, we define $\zeta \equiv \mathcal{F}_0/\mathcal{F}_C$ and study the regimes in which $\zeta < 1$ is valid. This criterion enables us to gauge the conditions under which Earth-like oxygenic photoautotrophs may have a low likelihood of existing. We only tackle the global average case herein, as it permits $\zeta < 1$ to occur in the parameter space. From examining Fig. 3, where the results are depicted, it is apparent that some tidally locked late-type M-dwarf exoplanets might be incapable of hosting phytoplankton-like biota. In particular, for the upper bound of $T_W = 50°$C, we surmise that stars with $T < 3150$ K can be ruled out in this category. Thus, if the oceans are sufficiently warm, tidally locked Earth-analogues around late-type M dwarfs could encounter difficulties in sustaining marine photosynthetic organisms analogous to modern Earth.

Lastly, before proceeding further, there is one other point worth mentioning. As the depth of the photosynthesis zone grows more shallower, whether it be due to oceanic temperature or stellar spectral type, the photoautotrophs are expected to live closer to the surface.

---

[4]We reiterate that our analysis deals with Earth-like biota, and the results are not necessarily applicable to putative oxygenic photoautotrophs in the oceans of M-dwarf exoplanets.

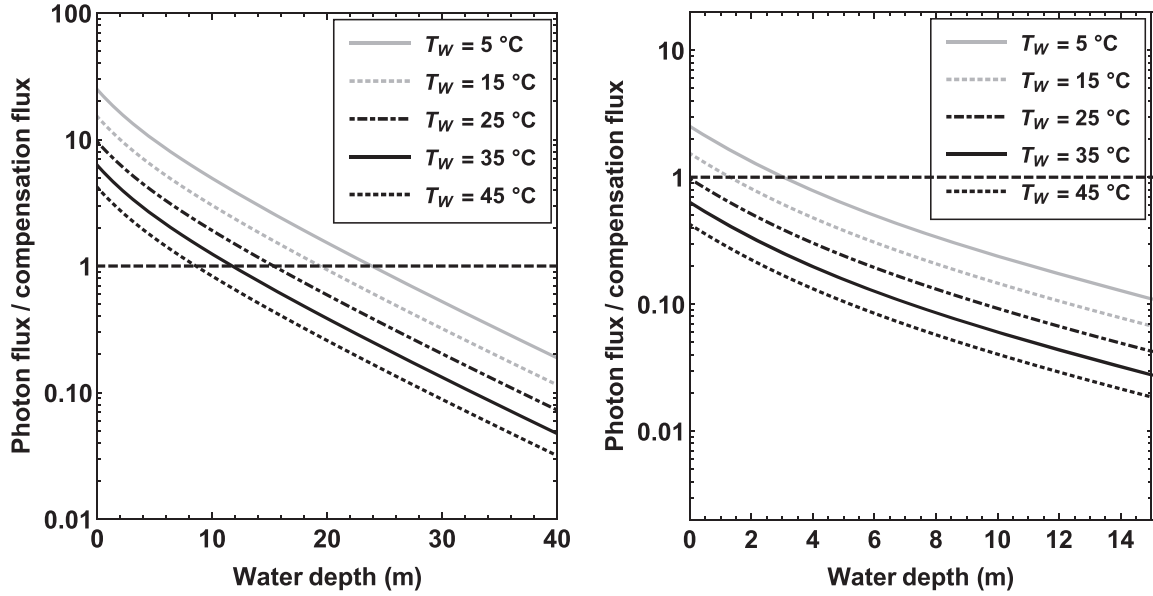[3]https://www.ncdc.noaa.gov/sotc/global/201913.

Figure 2. In both panels, the photon flux in units of the compensation flux is shown as a function of the ocean depth for the global average case described in Section 2; the compensation flux specifies the photon flux at which the net growth of the organism is not feasible. The various curves correspond to different choices of the global ocean temperature, and the intersection points of the various curves with the dashed horizontal line yield the compensation depths. The left- and right-hand panels correspond to Planets G and M, respectively, introduced in Section 2; for Planet M, the global average encapsulates the properties on the dayside.
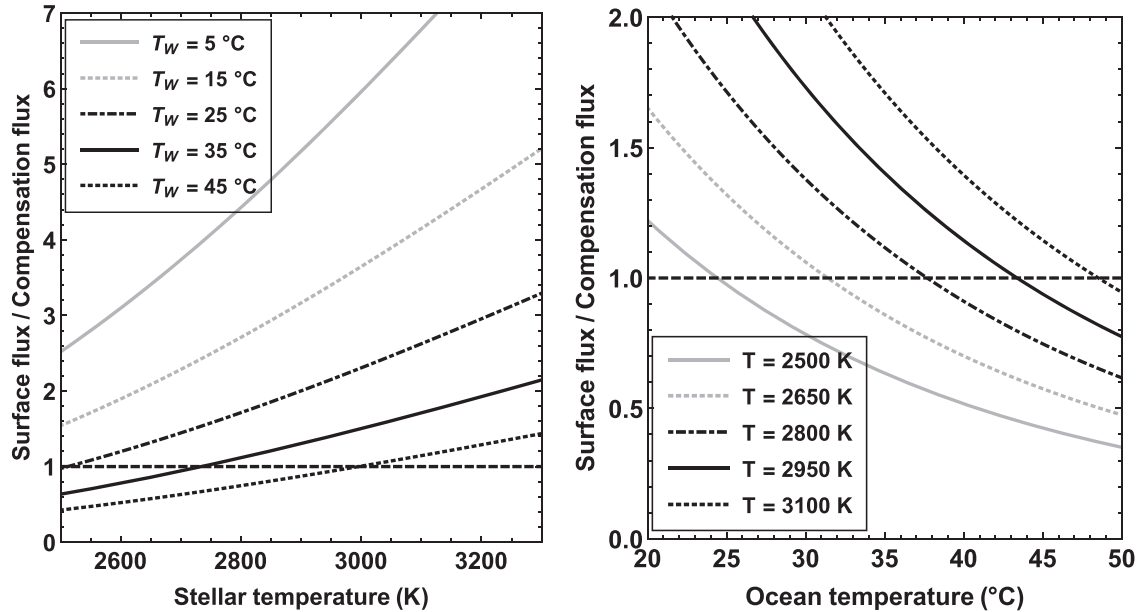

Figure 3. In both panels, the ratio of the photon flux at the surface to that of the compensation flux (denoted by ζ) is depicted. Regions lying below the horizontal dashed line are relatively unlikely to host Earth-like biota in the oceans. Left-hand panel: variation of ζ with stellar temperature (in K) for different ocean temperatures. Right-hand panel: variation of ζ with ocean temperature (in °C) for different stellar temperatures.

In doing so, they incur a greater risk of damage by ultraviolet radiation and energetic particles from flares and superflares, the latter of which could deposit high doses (Lingam & Loeb 2017; Yamashiki et al. 2019; Atri 2020). However, experiments and numerical models suggest that hazes (in)organic films (Cleaves & Miller 1998; Estrela & Valio 2018; Lingam & Loeb 2019b), along with biogenic ultraviolet screening compounds and evolutionary adaptations (Cockell & Knowland 1999; Abrevaya et al. 2020), may suffice to protect them.

3.2 Critical depth

In order to calculate the critical depth ($\mathcal{Z}_{CR}$), a number of different formulas have been delineated in the literature (Sverdrup 1953; Kirk 2011; Middelburg 2019). Most of the simpler models reduce to (equation 9.7 in Falkowski & Raven 2007)

$$K \mathcal{Z}_{CR} \approx \frac{\Gamma_P}{\Gamma_R}, \qquad (12)$$

but they are correct only in the limiting case of $K = \text{const}$, which is manifestly invalid. The generalization of the above equation was adumbrated in Lingam & Loeb ([2020b](#)), who eventually obtained

$$\mathcal{Z}_{\text{CR}} \approx \left(\frac{\Gamma_{\text{R}}}{\Gamma_{\text{P}}} \right)^{-1} \frac{\int_{\lambda_{\min}}^{\lambda_{\max}} \left[\mathcal{N}_0(\lambda)/K(\lambda) \right] \, d\lambda}{\int_{\lambda_{\min}}^{\lambda_{\max}} \mathcal{N}_0(\lambda) \, d\lambda}. \tag{13}$$

It is, however, necessary to recognize that $\Gamma_{\text{R}}/\Gamma_{\text{P}}$ has an intrinsic temperature dependence, as seen from (9). Hence, we combine (13) with (9), thereby yielding

$$\mathcal{Z}_{\text{CR}} \approx \frac{3.36 \times 10^{-2}}{\mathcal{G}(T_W)} \frac{\int_{\lambda_{\min}}^{\lambda_{\max}} \left[\mathcal{N}_0(\lambda)/K(\lambda) \right] \, d\lambda}{\int_{\lambda_{\min}}^{\lambda_{\max}} \mathcal{N}_0(\lambda) \, d\lambda}, \tag{14}$$

where the normalization has been adopted based on the global value for phytoplankton in Earth's oceans (chapter 4.3 in Sarmiento & Gruber [2006](#)). The parameters pertaining to the 'A' scenario are adopted for the sake of comparison with prior empirical studies.

The temperature dependence of the critical depth is illustrated in Fig. [4](#). Two points that emerge from scrutinizing this figure. From the left-hand panel, we notice that the dependence on the stellar temperature is weak at any given ocean temperature. This result is consistent with Lingam & Loeb ([2020b](#)), and is mostly attributable to the fact that net growth primarily occurs in the upper layers and thus compensates for the regions with $z > \mathcal{Z}_{\text{CO}}$. However, when it comes to the ocean temperature, a much stronger variation of $\mathcal{Z}_{\text{CR}}$ is discerned. As we cover the entire ocean temperature range considered herein, we find that $\mathcal{Z}_{\text{CR}}$ changes by nearly an order of magnitude for any given stellar temperature (right-hand panel). For instance, after we specify $T = T_{\odot}$, the critical depth evolves from $\mathcal{Z}_{\text{CR}}^{(A)} \approx 416$ m at $T_W \approx 0°\text{C}$ to $\mathcal{Z}_{\text{CR}}^{(A)} \approx 45$ m at $T_W \approx 50°\text{C}$.

Therefore, it is conceivable that the ocean temperature plays a major role in regulating the critical depth on other worlds. In turn, this development suggests that T_W also acts as a key determinant of phenomena analogous to phytoplankton blooms, which may constitute viable temporal biosignatures as noted earlier.

3.3 Net primary productivity

The NPP is arguably one of the most crucial and informative properties of a biosphere as it quantifies the net amount of organic carbon synthesized via biological pathways after accounting for losses dues to respiration and other factors; we will express our results in units of g C m^{-2} h^{-1} for the NPP. The NPP is a reliable measure of the amount of organic C generated via photosynthesis, as the latter constitutes the dominant carbon fixation pathway (Berg [2011](#); Knoll [2015](#); Judson [2017](#); Bar-On et al. [2018](#)). A wide spectrum of models have been developed to model NPP, and comprehensive reviews can be found in Behrenfeld & Falkowski ([1997a](#)) and Falkowski & Raven ([2007](#), chapter 9).

We make use of Field et al. ([1998](#), equation 3) to calculate the NPP because this outwardly simple expression accounts for a number of environmental factors:

$$\text{NPP} = C_{\text{sur}} \times \mathcal{Z}_{\text{CO}}^{(A)} \times f(\text{PAR}) \times P_{\text{opt}}(T_W), \tag{15}$$

where C_{sur} is the chlorophyll concentration at the surface, $f(\text{PAR})$ embodies the fraction of the water column up to $\mathcal{Z}_{\text{CO}}^{(A)}$ where photosynthesis is light saturated, and $P_{\text{opt}}(T_W)$ is the optimal carbon fixation rate. There exists, however, an inherent crucial subtlety that needs to be spelt out here. In canonical versions of the above formula, $\mathcal{Z}_{\text{CO}}^{(A)}$ is replaced by the euphotic zone depth. However, as noted in Field et al. ([1998](#), pg. 237), the proper variable that ought to be deployed is the depth of the zone where positive NPP is feasible,

which is congruent with the definition of the compensation depth. On Earth, the euphotic zone depth (Lee et al. [2007](#)) and the compensation depth (Sverdrup et al. [1942](#); Middelburg [2019](#)) are roughly equal to one another, but the same relationship is not necessarily valid *a priori* for other worlds; even on Earth, the reliability of the euphotic zone as a measure of the photosynthesis zone has been called into question (Banse [2004](#); Marra et al. [2014](#)).

The NPP will depend not only on the stellar and ocean temperatures but also on inherent biological factors such as C_{sur} that are spatially and temporally very heterogeneous. As the goal of this paper is to construct heuristic global estimates, we rewrite (15) so that it yields the average global value for the Earth at $T = T_{\odot}$ and $T_W = T_0$ (i.e. the parameters for Earth). By adopting the normalization from Field et al. ([1998](#)),[5] we obtain

$$\text{NPP} \approx 1.5 \times 10^{-2} \, \text{g C m}^{-2} \, \text{h}^{-1} \left(\frac{\mathcal{Z}_{\text{CO}}^{(A)}}{\mathcal{Z}_0} \right)$$
$$\times \mathcal{P}(T_W) \left(\frac{\mathcal{D}}{0.5} \right) \left(\frac{G(T)}{G(T_{\odot})} \right), \tag{16}$$

where $\mathcal{Z}_0 \approx 19$ m represents the compensation depth calculated at the fiducial ocean temperature of T_0 using the methodology in Section 3.1, while $\mathcal{D}$ denotes the fraction of time that a given location receives stellar illumination. For planets like Earth, we expect $\mathcal{D} \approx 0.5$ (i.e. equipartition of day and night) whereas tidally locked planets ought to have $\mathcal{D} \approx 1$ on the dayside because they receive stellar radiation *in perpetuo*. The auxiliary functions $G(T)$ and $\mathcal{P}(T_W)$ are defined as follows:

$$G(T) = \frac{\mathcal{F}_0}{\mathcal{F}_0 + \mathcal{F}_{\text{S}}}, \tag{17}$$

where $\mathcal{F}_{\text{S}} \approx 1.1 \times 10^3 \, \mu\text{mol m}^{-2} \, \text{s}^{-1}$, and the stellar temperature is implicitly present via $\mathcal{F}_0$:

$$\mathcal{P}(T_W) = \left[\frac{1 + \exp\left[\frac{E_{\text{h}}}{k_{\text{B}}} \left(\frac{1}{T_{\text{h}}} - \frac{1}{T_0} \right) \right]}{1 + \exp\left[\frac{E_{\text{h}}}{k_{\text{B}}} \left(\frac{1}{T_{\text{h}}} - \frac{1}{T_W} \right) \right]} \right]$$
$$\times \exp\left[\frac{E_{\text{a}}}{k_{\text{B}}} \left(\frac{1}{T_0} - \frac{1}{T_W} \right) \right], \tag{18}$$

where $E_{\text{a}} \approx 0.74$ eV, $E_{\text{h}} \approx 6.10$ eV, and $T_{\text{h}} \approx 34°\text{C}$ are adopted for our putative biota from Barton et al. ([2020](#), pg. 726).[6] Here, we have constructed (16) and (17) based on Behrenfeld et al. ([2005](#), section 2.4) and Behrenfeld & Falkowski ([1997a](#), equation 10), but a notable point of divergence is that a modified Sharpe–Schoolfield equation (Sharpe & DeMichele [1977](#); Schoolfield, Sharpe & Magnuson [1981](#)) is utilized as a proxy for $P_{\text{opt}}(T_W)$, following Barton & Yvon-Durocher ([2019](#)) and Barton et al. ([2020](#)) in lieu of Behrenfeld & Falkowski ([1997a](#), equation 11), as the latter becomes invalid for $T_W > 30°\text{C}$. The precise expression for $P_{\text{opt}}(T_W)$ for phytoplankton is challenging to accurately pin down, owing to the panoply of expressions used to model phytoplankton growth (Grimaud et al. [2017](#)). In consequence, a diverse array of functions, some exhibiting

---

[5]We note that some subsequent estimates for the oceanic NPP have revised the classic analysis of Field et al. ([1998](#)) by $\mathcal{O}(10$ per cent; Westberry et al. [2008](#)), but this has a minimal impact on both our subsequent qualitative and quantitative results.

[6]It goes without saying that all of these parameters exhibit substantive variation across species. For instance, the thermal performance curves for certain species of marine phytoplankton reveal optimal temperatures of $\sim 20°$–$25°\text{C}$ (Boyd et al. [2013](#)), in which case T_{h} is lowered by several $°\text{C}$.
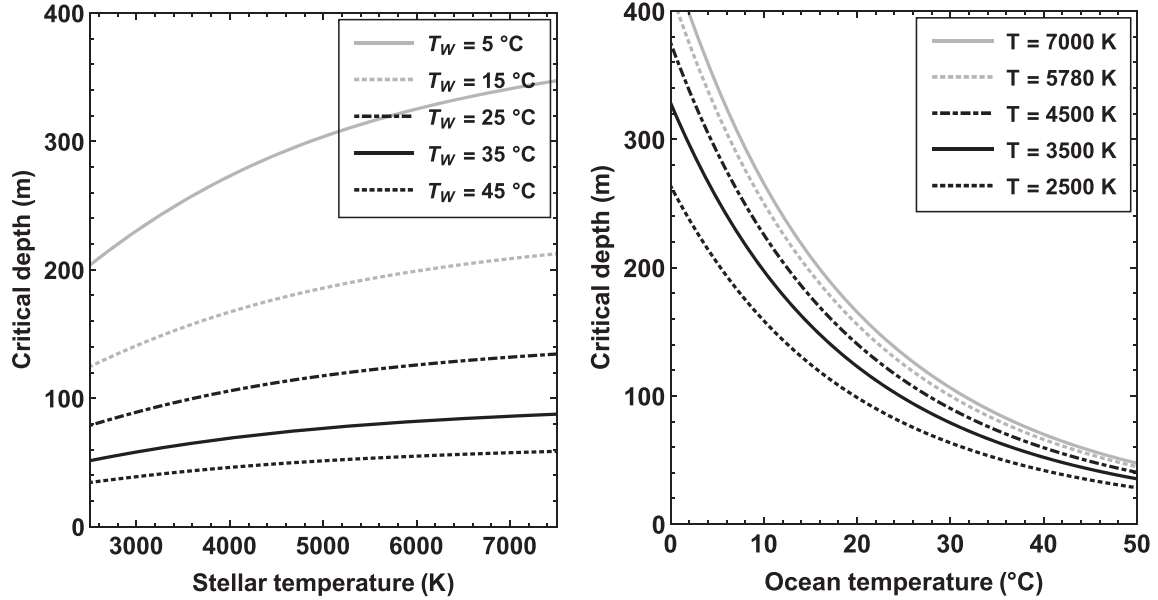
Figure 4. In both panels, the critical depth ($\mathcal{Z}_{CR}$) – to wit, the location where the vertically integrated net growth rate is zero – is plotted. Left-hand panel: variation of $\mathcal{Z}_{CR}$ with stellar temperature (in K) depicted for different ocean temperatures. Right-hand panel: variation of $\mathcal{Z}_{CR}$ with ocean temperature (in °C) illustrated for different stellar temperatures.

Table 1. Net primary productivity for the Earth-analogues as a function of the mean oceanic temperature.

Ocean temperature (° C)	Relative NPP of Planet G	Relative NPP of Planet M
5	0.4	9×10^{-3}
10	0.6	10^{-2}
15	0.9	10^{-2}
20	1.4	8×10^{-3}
25	2.0	0
30	2.7	0
35	1.2	0
40	6×10^{-2}	0
45	2×10^{-3}	0

*Note*s. The NPP is expressed in terms of the temporally averaged value associated with modern Earth's oceans, namely, $1.5 \times 10^{-2}\,\mathrm{g\,C\,m^{-2}\,h^{-1}}$. The NPP for these two Earth-analogues is calculated by deploying (16). Planet G orbits a solar twin whereas Planet M is situated near a late-type M dwarf akin to TRAPPIST-1; the other properties of the two planets are otherwise identical.

exactly opposite trends with temperature, have been employed for this purpose (fig. 4 in Behrenfeld & Falkowski 1997b); see also Grimaud et al. (2017). Hence, the ensuing results should be interpreted with due caution.

We have presented the NPP for the two Earth-analogues (Planet G and Planet M) in Table 1 and Fig. 5, which were calculated by using the global average case as seen from (15). There are several interesting results that emerge from inspecting these two items. We begin by considering Planet G (orbiting a solar twin) to gauge the role of T_W. We notice that the NPP increases with ocean temperature until $\sim 30°$C, but the growth is relatively modest. It is primarily driven by the rise in the rate of carbon fixation, as encapsulated by $\mathcal{P}(T_W)$, with temperature in this regime. In some controlled experiments and modelling where the temperature was steadily elevated, the photosynthetic capacity has been found to increase up to a point
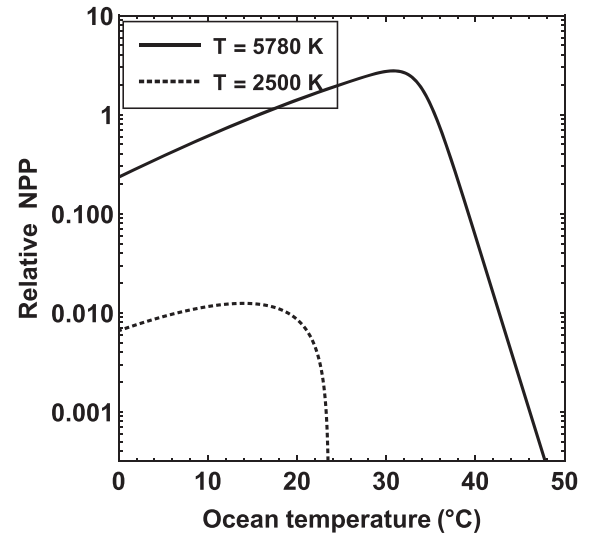

Figure 5. The oceanic NPP relative to that of modern Earth as a function of the ocean temperature for Planets G (stellar temperature of $T = 5780$ K) and M (stellar temperature of $T = 2500$ K).

(Lewandowska et al. 2014; Padfield et al. 2016; Schaum et al. 2017).[7] As per our simple model, once the peak temperature of the thermal performance curve is exceeded (T_{pk}), the rate of carbon fixation falls sharply thereafter, and consequently drives the steep decline in NPP when $T_W > 35°$C.

Now, we turn our attention to Planet M around a late-type M dwarf similar to TRAPPIST-1. For any fixed temperature, say $T_W =$

---

[7]It is important to recognize, however, that the variation of NPP with temperature is subject to much uncertainty due to the large number of coupled variables and non-linear feedback mechanisms (Taucher & Oschlies 2011; Laufkötter et al. 2015).

5°C, we notice that the NPP is lower than Planet G by roughly two orders of magnitude. The reasons for the diminished NPP are twofold: (i) the compensation depth is greatly reduced as pointed out in Section 3.1, and (ii) the flux of PAR is corresponding lower at the surface, thereby making the last term on the right-hand-side of (16) smaller than unity. The next major feature we notice is that the NPP vanishes at $T_W \sim 24$°C. This result is a direct consequence of the fact that the compensation depth becomes zero above a threshold temperature for reasons explained in Section 3.1. Hence, tidally locked exoplanets around late-type M dwarfs may evince a low likelihood of large-scale carbon fixation by phytoplankton-like biota. Needless to say, the NPP is not anticipated to be zero *sensu stricto* because anoxygenic photoautotrophs are capable of carbon fixation by definition (Konhauser 2007; Schlesinger & Bernhardt 2013), and so are many microbial taxa in the deep biosphere (Orcutt et al. 2011; Edwards, Becker & Colwell 2012; McMahon & Parnell 2014; Colman et al. 2017).

4 LIMITATIONS OF THE MODEL

It is worth emphasizing at the outset that the productivity of biospheres is constrained by a number of factors including water, electron donors, temperature, PAR flux, and nutrients (Lingam & Loeb 2021). Our analysis tackles the modulation of the productivity of biospheres by PAR and ambient ocean temperature *ceteris paribus*. In doing so, we follow the likes of Lehmer et al. (2018) and Lingam & Loeb (2019d) in setting aside the constraints imposed by the access to nutrients and some of the other variables.

In the case of Earth's terrestrial (land-based) NPP, the NPP for > 80 per cent of the area is limited by water and temperature (Churkina & Running 1998). In contrast, Earth's oceanic NPP – both the globally averaged value and the spatiotemporal variations – is governed by the prevalence of nutrients, especially the ultimate limiting nutrient phosphate (Tyrrell 1999; Filippelli 2008; Schlesinger & Bernhardt 2013). Ocean planets, in particular, may be impacted due to their potentially lower rates of weathering and delivery of nutrients to the oceans (Wordsworth & Pierrehumbert 2013; Lingam & Loeb 2018b,c; Kite & Ford 2018). The key caveat in this paper, therefore, is that the oceanic NPP is not constrained by nutrients, but is instead regulated the two factors adumbrated in the preceding paragraph. The ensuing results might comprise upper bounds for the NPP because the abundance and distribution of nutrients could introduce additional limits.

As we demonstrated in Section 3.3, the oceanic NPP for tidally locked Earth-like exoplanets around late-type M dwarfs is severely constrained by the paucity of PAR photons, and is orders of magnitude smaller than Earth's oceanic NPP. Hence, the prior assumption might not pose a major problem for these worlds because the most dominant bottleneck on the oceanic NPP may prove to be the PAR flux. However, when it comes to Earth-analogues around Sun-like stars, PAR flux is not a major limiting factor and the thermal effects on NPP might become prominent only at high temperatures. Thus, a brief discussion of nutrient limitation and how it could impact the oceanic NPP of other worlds is apropos.

The first and foremost point that needs to be appreciated is that modelling nutrient limitation even on Earth is a complicated endeavor. The reason is that the nutrient concentration in the ocean depends on a variety of factors such as the remineralization efficiency (Kipp & Stüeken 2017; Laakso & Schrag 2018), hydrothermal activity (Wheat, Feely & Mottl 1996), submarine weathering (Hao et al. 2020), and mineral solubility in seawater (Derry 2015), to name just a few. Moreover, each of these quantities has fluctuated over

time and witnessed shifts in magnitude, sometimes up to a factor of ~10 as may have occurred vis-à-vis the remineralization efficiency during the Ediacaran period (Laakso et al. 2020). For these reasons, theoretical models for the biogeochemical cycles of the bioessential elements have yielded very different results (Lenton 2020); see also Hao et al. (2020) for an exposition of this issue.

As the prior discussion suggests, there are numerous mechanisms that control the nutrient concentration in oceans. In consequence, it is not inconceivable that some Earth-like planets could bypass or mitigate the issue of nutrient limitation. Geological processes that have been proposed hitherto for counteracting the nutrient deficiency to varying degrees include elevated nutrient upwelling (Lingam & Loeb 2018a; Olson et al. 2020; Salazar et al. 2020), submarine basalt weathering (Syverson et al. 2020), and serpentinization (Pasek et al. 2020). As noted earlier, we presumed that nutrient abundance is not the chief limitation, perhaps via some of the above channels coming into play. To reiterate, we supposed that either photon flux and/or temperature act to throttle the productivity. We have consequently demonstrated that these factors become exceedingly important for planets around late-type M dwarfs and/or with high ambient ocean temperatures; in particular, the NPP might become orders of magnitude smaller relative to Earth.

In relation to the preceding points, we note that the constraints imposed by the ambient photon flux, temperature and nutrients do not act independently of one another. In fact, a multitude of experiments and field studies have established that these environmental parameters are non-linearly coupled to one another (Edwards et al. 2016; Sinclair et al. 2016; Grimaud et al. 2017; Thomas et al. 2017; Marañón et al. 2018). For instance, the value of E_a introduced previously may vary significantly in some species depending on the availability of nitrogen (Marañón et al. 2018) and the ocean temperature (Mundim et al. 2020). While such effects are indubitably important, they are not well understood even on Earth and exhibit considerable intra- and inter-species variability. Hence, given that the implicit goal of this paper was to construct heuristic models that provide rough estimates for future observations and modelling, we have not taken these subtle processes into account.

Lastly, in our subsequent analysis, we drew upon the basic physiological properties of the dominant phytoplankton species on Earth. While this line of reasoning is undoubtedly parochial, we note that Earth-based organisms are commonly used as proxies in numerous astrobiological contexts (Martins et al. 2017), ranging from extremophiles and microbial ecosystems in the oceans of icy moons (Chyba & Hand 2001; Rothschild & Mancinelli 2001; Cottin et al. 2017; Martins et al. 2017; Merino et al. 2019; Lingam & Loeb 2019a) to the limits of complex multicellular life on exoplanets (Silva et al. 2017; Schwieterman et al. 2019; Lingam 2020; Ramirez 2020). Furthermore, the choice of phytoplankton as putative biota is motivated by the fact that they are the major source of carbon fixation in the oceans of modern Earth (Harris 1986; Falkowski et al. 2004; Canfield, Kristensen & Thamdrup 2005; Raven 2009; Uitz et al. 2010). Hence, by utilizing the prior framework, we are now equipped to analyse the prospects for Earth-like aquatic photosynthesis on other worlds characterized by different ocean temperatures.

5 DISCUSSION

We will discuss some of the implications of our work in connection with mapping the trajectories of the Earth as well as tidally locked M-dwarf exoplanets.

5.1 Potential future evolution of Earth

We begin by tackling the ramifications of the preceding analysis for the Earth's aquatic biosphere, with respect to its potential future.

Before doing so, it is worth briefly highlighting the inherent spatiotemporal variability of Earth's oceanic NPP. To begin with, let us recall that a global sea surface temperature (SST) of $T_0 \approx 16°C$ was chosen herein based on satellite data. However, in reality, the SST of Earth is characterized by distinct heterogeneity, ranging from $35°C$ to below-freezing temperatures.[8] Moreover, the Earth's NPP is modulated by the access to not only light and temperature (both of which are present in our model) but also nutrients (Behrenfeld et al. 2005); the latter may play a crucial role as noted in Section 4. Collectively, these factors engender variations in the oceanic NPP across both the spatial and temporal domains (Westberry et al. 2008), sometimes by roughly an order of magnitude. Thus, we reiterate that our model only seeks to extract globally averaged values for the relevant variables from a heuristic standpoint.

There is a sharp downswing in NPP shortly after the peak temperature T_{pk} is attained, which becomes evident upon inspecting Fig. 5. While there are grounds for contending that $T_{pk} \sim 30°C$ (Barton et al. 2020), this matter is admittedly not conclusively settled. Now, let us suppose that the Earth's temperature was raised by $\sim 10°C$ abruptly. In large swathes of the ocean, it is conceivable that $T_W > T_{pk}$, thereby triggering a sharp downswing in the NPP in these regions. In turn, given that phytoplankton are the foundation of oceanic food webs and tropic interactions (Barnes & Hughes 1999; Valiela 2015; Kirchman 2018), this rapid decline in NPP ought to have adverse consequences for marine ecosystems and could thus potentially drive large-scale extinctions of marine biota.

As the Sun continues to grow brighter, the surface temperature will also increase commensurately because of the greenhouse effect until the Earth is eventually rendered uninhabitable (Caldeira & Kasting 1992; Goldblatt & Watson 2012; Rushby et al. 2013). Based on Wolf & Toon (2015, section 3.1), we note that a global temperature of 312 K is predicted when the solar luminosity is 1.1 times the present-day value. By utilizing Gough (1981, equation 1), the stellar luminosity associated with this temperature is expected to occur $\sim$1.2 Gyr in the future. It is important to note, however, that climate models do not fully agree on the critical flux at which the greenhouse state is likely to be activated, implying that a timescale of <1 Gyr ought not be ruled out (Goldblatt et al. 2013; Leconte et al. 2013; Kasting, Chen & Kopparapu 2015; Popp, Schmidt & Marotzke 2016; Wolf et al. 2017).

If we suppose that the global ocean temperature tracks the average surface temperature, the above analysis suggests that $T_W \sim 39°C$ would occur $\sim$1.2 Gyr hereafter. After examining Fig. 5, we find that the oceanic NPP at this T_W might be < 10 per cent of modern Earth. Due to the diminished NPP, eventual depletion of atmospheric O_2 is plausible for reasons adumbrated in Section 5.2, namely, when the sinks for oxygen outpace the sources. A decline in atmospheric O_2 could, in turn, drive the extinction of motile macroscopic organisms, as their long-term survival customarily necessitates oxygen levels $\sim$ 10 per cent of their present value (Catling et al. 2005; Willmer, Stone & Johnston 2005; Zhang & Cui 2016; Reinhard et al. 2016).[9] Thus, *in toto*, the biosphere is unlikely to exhibit the same

complexity as that of present-day Earth: this qualitative result is broadly consistent with earlier predictions by O'Malley-James et al. (2013, 2014).

5.2 Tidally locked M-dwarf exoplanets

We turn our attention to Planet M, i.e. the putative tidally locked exoplanet around a late-type M dwarf similar to TRAPPIST-1.

It is instructive to compare our results against prior analyses of related topics. Wolstencroft & Raven (2002, table A9) calculated the oceanic NPP, albeit at a fixed depth of 10 m using a simple model based on the photon flux, and estimated that it was approximately five times lower for an Earth-analogue around an M0 star. In a similar vein, Lehmer et al. (2018) and Lingam & Loeb (2019d) employed simple models for the NPP that were linearly proportional to the incident photon flux and determined that planets orbiting late-type M dwarfs are unlikely to host biospheres with the same NPP as modern Earth and build up atmospheric O_2 to detectable levels. Thus, by and large, our work maintains consistency with earlier studies, but it has taken several other environmental and physiological variables into account that were missing in previous analyses.

We have previously calculated that the NPP for Planet M is, at most, only a few per cent of the Earth's current oceanic NPP. Hence, because of the low NPP, unless the burial efficiency of organic carbon is unusually high, it seems likely that the flux of O_2 contributed by oxygenic photosynthesis will be correspondingly small. Hence, it ought to become more feasible for the sinks of atmospheric O_2 (e.g. continental weathering and volcanic outgassing) to dominate this source (which is a major player on Earth). The end result is that O_2 has a low likelihood of accumulating to detectable levels in the atmosphere (Catling & Kasting 2017).

This potential effect has two consequences in turn. First, O_2 has been conjectured to be an essential prerequisite for complex life insofar as metabolism is concerned (Knoll 1985; McKay 1996; Catling et al. 2005; Lingam & Loeb 2021), at least up to a certain threshold after which oxygen toxicity may set in (Lingam 2020). Hence, the evolution of complex life, and potentially technological intelligence, might be suppressed on this category of worlds. Secondly, and more importantly, the absence of detectable atmospheric O_2 or O_3 for the aforementioned reasons despite the existence of a biosphere is an archetypal example of a 'false negative' that can hinder or complicate the search for extraterrestrial life (Reinhard et al. 2017; Meadows et al. 2018).

5.3 Build-up of atmospheric oxygen on ocean worlds

It is worth quantifying the above qualitative treatment to gain further insights for ocean planets that are otherwise akin to present-day Earth. We will adopt the prescription laid out in Lehmer et al. (2018). We begin the analysis by noting that Earth's current oceanic NPP translates to an O_2 production flux of 5×10^{-4} mol m^{-2} h^{-1}, because the simplified reaction scheme for oxygenic photosynthesis takes the form

$$CO_2 + 2H_2O \xrightarrow[\text{pigments}]{h\nu} CH_2O + H_2O + O_2, \tag{19}$$
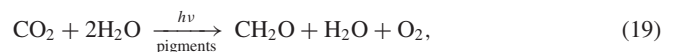
where CH_2O embodies the synthesis of organic compounds, and H_2O appears in both sides of the equation as reactant and product, respectively. However, only a minuscule fraction of this O_2 is deposited in the atmosphere, since the vast majority is consumed by respiration and oxidative decay. If we denote the burial fraction

---

[8]https://earthobservatory.nasa.gov/global-maps/MYD28M

[9]In contrast, relatively sessile animals, such as the demosponge *Halichondria panicea* (Mills et al. 2014), are capable of surviving at oxygen levels around two to three orders of magnitude smaller than today (Sperling, Knoll & Girguis 2015; Leys & Kahn 2018).

by ϕ, the flux of O_2 produced is then given by

$$\dot{S} \sim 1.5 \times 10^{-6} \, \text{mol m}^{-2} \, \text{h}^{-1} \left(\frac{\text{NPP}}{\text{NPP}_\oplus} \right) \left(\frac{\phi}{\phi_\oplus} \right), \qquad (20)$$

where $\dot{S}$ is the O_2 flux generated from organic carbon burial, $\text{NPP}_\oplus$ is the globally averaged oceanic NPP of the Earth, and $\phi_\oplus \approx 3 \times 10^{-3}$ is the fraction of organic carbon (fixed by photosynthesis) subjected to burial on present-day Earth (Holland 2002; Lehmer et al. 2018). In order for O_2 to build up on anoxic worlds, the above source must exceed the primary sink, namely, reducing gases arising from a mixture of surface and submarine volcanism, metamorphism and serpentinization to name a few (Catling & Kasting 2017). We introduce $\dot{D}$, the depletion flux of O_2 associated with reducing gases, and specify a fiducial value of $\dot{D}_\oplus \sim 1.3 \times 10^{-6} \, \text{mol m}^{-2} \, \text{h}^{-1}$ for modern Earth (Catling & Kasting 2017). The criterion for O_2 accumulation in the atmosphere is thus expressible as $\dot{S} > \dot{D}$, which simplifies to

$$\text{NPP} > 0.9 \text{NPP}_\oplus \left(\frac{\phi}{\phi_\oplus} \right)^{-1} \left(\frac{\dot{D}}{\dot{D}_\oplus} \right). \qquad (21)$$

Hence, the above relation suggests that the oceanic NPP must be close to its present-day value in order for the build up of atmospheric O_2 to potentially take place, if all other parameters are held fixed. In contrast, if the burial of carbon is very efficient or the flux of reducing gases is extremely low, even a NPP that is much smaller than that of modern Earth may support the accumulation of atmospheric O_2. We run into an immediate difficulty here since both ϕ and $\dot{D}$ are not tightly constrained for Earth-like worlds in general.

However, if we interpret Earth-analogues to include only those worlds with all geochemical parameters similar to Earth, we can make headway. In such cases, (21) reduces to the simpler NPP > $0.9 \text{NPP}_\oplus$. By comparing this criterion with Fig. 5, it is possible to deduce the conditions that permit the build up of atmospheric O_2 if only light and temperature constitute the sole limiting factors (cf. the next paragraph). For Earth-analogues around solar twins, we find that a temperature range of $\sim 15^\circ$–35°C might permit the build up of atmospheric O_2. At much higher and lower temperatures, the NPP is accordingly diminished, owing to which the reducing gases could overwhelm the O_2 generated from carbon burial. When we consider tidally locked Earth-analogues around late-type M dwarfs, Fig. 5 and Table 1 suggest that the NPP would be only a few per cent of Earth's current oceanic NPP. In that event, it might not be feasible for the accumulation of atmospheric O_2 to occur, as per the simplified formalism we have adopted.

5.4 Observational tests for the future

It is helpful to examine the prospects for testing our results by means of future observations at this juncture. A number of publications mentioned at the beginning of Section 5.2 have already propounded strategies to gauge whether the stellar spectral type affects the NPP and the accompanying rise in atmospheric O_2 levels. The basic idea is to search for correlations between the spectral type of the host star on the one hand and the presence/absence of O_2 on the other. However, these putative correlations need to be weighed carefully because of the presence of major sources and sinks of O_2 not prevalent on Earth; for instance, the abiotic build-up of O_2 may be driven by electromagnetic radiation (Wordsworth & Pierrehumbert 2014; Luger & Barnes 2015; Harman et al. 2015; Kleinböhl et al. 2018) or its depletion may be effectuated by intense stellar winds and space weather events (Garcia-Sage et al. 2017; Dong et al. 2017a,b,

2018a,b; Dong, Huang & Lingam 2019; Dong, Jin & Lingam 2020; Airapetian et al. 2020).

Therefore, we will restrict ourselves to assessing the observational implications insofar as worlds with varying ocean temperature are concerned. A scrutiny of Fig. 5 reveals that a fairly steep decline in the NPP is potentially anticipated above a certain cutoff temperature. On the other hand, the surface density of chlorophyll (C_{sur}) appearing in (15) might not be affected to the same degree; in fact, we have held it fixed for the sake of simplicity. Hence, at least in principle, the detection of photoautotrophs ought to be feasible via the photosynthetic red edge (Seager et al. 2005), especially in the event that the organisms cover a large fraction of the surface (O'Malley-James & Kaltenegger 2019).

If we can therefore sample enough planets and discern a critical mean ocean temperature (the surface temperature might comprise a rough proxy for T_W) for a particular spectral type above which no biogenic O_2 and O_3 are detected but a tangible photosynthetic red edge is identified, such a distinct correlation could provide an avenue for gauging our hypothesis. However, we caution that this strategy is not easily implementable in the near-future because it necessitates access to a sufficiently large sample of worlds with confirmed reliable biosignatures, oceans, and surface temperature measurements (Kaltenegger 2017; Schwieterman et al. 2018; Fujii et al. 2018; Madhusudhan 2019).

6 CONCLUSIONS

In this paper, we investigated how the ambient ocean temperature T_W and the spectral type of the host star may influence the characteristics of aquatic biospheres on Earth-like worlds, albeit under a set of key assumptions that were expounded in Section 4.

In spite of the underlying simplifications and the ensuing limitations, there are several new results that were presented in this work, of which some of the major ones are outlined below and described in more detail later:

(i) The compensation depth and critical depth is calculated as a function of the mean ocean temperature for Earth-analogues around a late-type M dwarf (Planet M) and a Sun-like star (Planet G); it should be noted that Planet M is modelled as being tidally locked.

(ii) The *vertically integrated* average oceanic NPP is estimated for Planet G and Planet M. In other words, the procedure for determining the oceanic NPP as a function of the spectral type and the ocean temperature was explicated.

(iii) The criterion for the accumulation of oxygen (O_2) in the atmospheres of Planets G and M is derived; this criterion is dependent not only on the spectral type but also on the ocean temperature.

We began by estimating the compensation depth and critical depth, as they serve to quantify the depths at which the net growth rate and vertically integrated net growth rate become zero, respectively. We showed that the ocean temperature has a relatively moderate influence on the compensation depth for an Earth-analogue around a solar twin, as $\mathcal{Z}_{\text{CO}}$ varies only by a factor less than 3. In contrast, when it comes to an Earth-like tidally locked world orbiting a late-type M dwarf akin to TRAPPIST-1, we found that T_W causes $\mathcal{Z}_{\text{CO}}$ to vary by at least an order of magnitude. Furthermore, sufficiently warm oceans may preclude phytoplankton-like biota from existing on these worlds altogether. We calculated the critical depth and showed that it is sensitive to T_W, and varies by nearly an order of magnitude for the temperature range considered herein.

Next, we examined the oceanic NPP of Planet G and Planet M as a function of the ocean temperature. The NPP constitutes one of the most vital metrics for a biosphere, and it has practical consequences that are delineated in the next paragraph. This calculation entailed the estimation of several variables, of which a few have not been robustly determined as empirical functions of T_W. Bearing this caveat in mind, we found that the NPP on Planet G was not very sensitive to T_W until it exceeded a certain threshold after which the rate of carbon fixation dropped precipitously and drove a corresponding decline in the NPP. For the case of Planet M, the NPP was determined to be $\lesssim 1$ per cent that of modern Earth, primarily on account of the shallowness of the photosynthesis zone in tandem with the lower PAR fluxes. When the ocean temperatures were raised sufficiently, the conditions for phytoplankton-like biota became untenable as noted in the earlier paragraph, and consequently resulted in the NPP approaching zero.

Lastly, we analysed the ramifications of our work in the context of our planet as well as tidally locked Earth-like exoplanets orbiting late-type M dwarfs. We discussed how an increase of $\sim 10^\circ$C in the ocean temperature, such as what is expected to happen $\lesssim 1$ Gyr in Earth's future due to the growing solar luminosity, could radically transform the aquatic biosphere of Earth-analogues around G-type stars and diminish the NPP to < 10 per cent of the Earth's current oceanic NPP in large swathes of the oceans. In a similar vein, we surmised that the aquatic biospheres of tidally locked Earth-like worlds around late-type M dwarfs may evince NPPs that are $\lesssim 1$ per cent of our planet's oceanic NPP today. If this prediction is correct, these worlds would be unlikely to accumulate atmospheric O_2 – except in circumstances where they have much higher carbon burial and lower outgassing of reducing gases – but signatures of life are nonetheless potentially detectable through the photosynthetic red edge if the coverage and density of photoautotrophs is high enough. We concluded our discussion by sketching rubrics which might enable the behaviour of NPP with spectral type and temperature to be gauged by future observations.

ACKNOWLEDGEMENTS

DATA AVAILABILITY STATEMENT

No new data were generated or analysed in support of this research.

REFERENCES

Abbot D. S., Cowan N. B., Ciesla F. J., 2012, ApJ, 756, 178
Abrevaya X. C., Leitzinger M., Oppezzo O. J., Odert P., Patel M. R., Luna G. J. M., Forte Giacobone A. F., Hanslmeier A., 2020, MNRAS, 494, L69
Airapetian V. S. et al., 2020, Int. J. Astrobiol., 19, 136
Angilletta M. J., 2009, Thermal Adaptation: A Theoretical and Empirical Synthesis. Oxford Univ. Press, Oxford
Arndt N. T., Nisbet E. G., 2012, Annu. Rev. Earth Planet. Sci., 40, 521
Atri D., 2020, MNRAS, 492, L28
Banse K., 2004, Limnol. Oceanogr. Bull., 13, 49
Bar-On Y. M., Phillips R., Milo R., 2018, Proc. Natl. Acad. Sci., 115, 6506
Barnes R., 2017, Celest. Mech. Dyn. Astron., 129, 509
Barnes R. S. K., Hughes R. N., 1999, An Introduction to Marine Ecology, 3rd edn. Blackwell Publishing, Oxford
Barton S., Yvon-Durocher G., 2019, Limnol. Oceanogr., 64, 2081
Barton S., Jenkins J., Buckling A., Schaum C.-E., Smirnoff N., Raven J. A., Yvon-Durocher G., 2020, Ecol. Lett., 23, 722
Behrenfeld M. J., 2010, Ecology, 91, 977
Behrenfeld M. J., Boss E. S., 2018, Glob. Change Biol., 24, 55
Behrenfeld M. J., Falkowski P. G., 1997a, Limnol. Oceanogr., 42, 1
Behrenfeld M. J., Falkowski P. G., 1997b, Limnol. Oceanogr., 42, 1479
Behrenfeld M. J., Boss E., Siegel D. A., Shea D. M., 2005, Global Biogeochem. Cy., 19, GB1006
Berg I. A., 2011, Appl. Environ. Microbiol., 77, 1925
Blankenship R. E., 2014, Molecular Mechanisms of Photosynthesis, 2nd edn. Wiley-Blackwell, Chichester
Boyd P. W. et al., 2013, PLoS One, 8, e63091
Brown J. H., Gillooly J. F., Allen A. P., Savage V. M., West G. B., 2004, Ecology, 85, 1771
Bruno J. F., Carr L. A., O'Connor M. I., 2015, Ecology, 96, 3126
Caldeira K., Kasting J. F., 1992, Nature, 360, 721
Canfield D., Kristensen E., Thamdrup B., 2005, Aquatic Geomicrobiology. Academic Press, Amsterdam
Catling D. C., Kasting J. F., 2017, Atmospheric Evolution on Inhabited and Lifeless Worlds. Cambridge Univ. Press, Cambridge
Catling D. C., Glein C. R., Zahnle K. J., McKay C. P., 2005, Astrobiology, 5, 415
Checlair J. H., Olson S. L., Jansen M. F., Abbot D. S., 2019, ApJ, 884, L46
Chen M., Blankenship R. E., 2011, Trends Plant Sci., 16, 427
Chen J., Kipping D., 2017, ApJ, 834, 17
Chiswell S., 2011, Mar. Ecol. Prog. Ser., 443, 39
Churkina G., Running S. W., 1998, Ecosystems, 1, 206
Chyba C. F., Hand K. P., 2001, Science, 292, 2026
Clarke A., 2014, Int. J. Astrobiol., 13, 141
Clarke A., 2017, Principles of Thermal Ecology: Temperature, Energy and Life. Oxford Univ. Press, Oxford
Claudi R. et al., 2021, Life, 11, 10
Cleaves H. J., Miller S. L., 1998, Proc. Natl. Acad. Sci., 95, 7260
Cockell C. S., 2020, Astrobiology: Understanding Life in the Universe, 2nd edn. John Wiley & Sons, Hoboken
Cockell C. S., Knowland J., 1999, Biol. Rev., 74, 311
Cockell C. S. et al., 2016, Astrobiology, 16, 89
Colman D. R., Poudel S., Stamps B. W., Boyd E. S., Spear J. R., 2017, Proc. Natl. Acad. Sci., 114, 6895
Corkrey R., McMeekin T. A., Bowman J. P., Olley J., Ratkowsky D., 2018, Int. J. Astrobiol., 17, 17
Cossins A. R., Bowler K., 1987, Temperature Biology of Animals. Chapman & Hall, London
Cottin H. et al., 2017, Space Sci. Rev., 209, 83
Cowan N. B., Abbot D. S., 2014, ApJ, 781, 27
Cullum J., Stevens D. P., 2016, Proc. Natl. Acad. Sci., 113, 4278
Deamer D., Weber A. L., 2010, Cold Spring Harb. Perspect. Biol., 2, a004929
Del Genio A. D., Way M. J., Kiang N. Y., Aleinov I., Puma M. J., Cook B., 2019, ApJ, 887, 197
Dell A. I., Pawar S., Savage V. M., 2011, Proc. Natl. Acad. Sci., 108, 10591
Delrez L. et al., 2018, MNRAS, 475, 3577
Derry L. A., 2015, Geophys. Res. Lett., 42, 8538
Dole S. H., 1964, Habitable Planets for Man. Blaisdell, New York
Dong C., Lingam M., Ma Y., Cohen O., 2017a, ApJ, 837, L26
Dong C., Huang Z., Lingam M., Tóth G., Gombosi T., Bhattacharjee A., 2017b, ApJ, 847, L4
Dong C., Jin M., Lingam M., Airapetian V. S., Ma Y., van der Holst B., 2018a, Proc. Natl. Acad. Sci., 115, 260
Dong C. et al., 2018b, ApJ, 859, L14
Dong C., Huang Z., Lingam M., 2019, ApJ, 882, L16
Dong C., Jin M., Lingam M., 2020, ApJ, 896, L24
Dorn C., Mosegaard K., Grimm S. L., Alibert Y., 2018, ApJ, 865, 20

Edwards K. J., Becker K., Colwell F., 2012, Annu. Rev. Earth Planet. Sci., 40, 551

Edwards K. F., Thomas M. K., Klausmeier C. A., Litchman E., 2016, Limnol. Oceanogr., 61, 1232

Ehlmann B. L. et al., 2016, J. Geophys. Res. Planets, 121, 1927

Estrela R., Valio A., 2018, Astrobiology, 18, 1414

Falkowski P. G., Raven J. A., 2007, Aquatic photosynthesis, 2nd edn. Princeton Univ. Press, Princeton

Falkowski P. G., Katz M. E., Knoll A. H., Quigg A., Raven J. A., Schofield O., Taylor F. J. R., 2004, Science, 305, 354

Field C. B., Behrenfeld M. J., Randerson J. T., Falkowski P., 1998, Science, 281, 237

Filippelli G. M., 2008, Elements, 4, 89

Fischer A. D., Moberg E. A., Alexander H., Brownlee E. F., Hunter-Cevera K. R., Pitz K. J., Rosengard S. Z., Sosik H. M., 2014, Oceanography, 27, 222

Flament N., Coltice N., Rey P. F., 2008, Earth Planet. Sci. Lett., 275, 326

Fujii Y. et al., 2018, Astrobiology, 18, 739

Gaarder T., Gran H. H., 1927, Rapp. Proc. Verb. Cons. Int. Explor. Mer, 42, 3

Gale J., Wandel A., 2017, Int. J. Astrobiol., 16, 1

Garcia-Sage K., Glocer A., Drake J. J., Gronoff G., Cohen O., 2017, ApJ, 844, L13

Gillon M. et al., 2017, Nature, 542, 456

Gillooly J. F., Brown J. H., West G. B., Savage V. M., Charnov E. L., 2001, Science, 293, 2248

Goldblatt C., 2015, Astrobiology, 15, 362

Goldblatt C., Watson A. J., 2012, Phil. Trans. R. Soc. A, 370, 4197

Goldblatt C., Robinson T. D., Zahnle K. J., Crisp D., 2013, Nat. Geosci., 6, 661

Gough D. O., 1981, Sol. Phys., 74, 21

Gran H. H., Braarud T., 1935, J. Biol. Bd Can., 1, 279

Grimaud G. M., Mairet F., Sciandra A., Bernard O., 2017, Rev. Environ. Sci. Biotechnol., 16, 625

Grimm S. L. et al., 2018, A&A, 613, A68

Hale G. M., Querry M. R., 1973, Appl. Opt., 12, 555

Hao J., Knoll A. H., Huang F., Schieber J., Hazen R. M., Daniel I., 2020, Geochim. Cosmochim. Acta, 280, 360

Harman C. E., Schwieterman E. W., Schottelkotte J. C., Kasting J. F., 2015, ApJ, 812, 137

Harris G., 1986, Phytoplankton Ecology: Structure, Function and Fluctuation. Chapman & Hall, London

Heller R., Armstrong J., 2014, Astrobiology, 14, 50

Hochachka P. W., Somero G. N., 2002, Biochemical Adaptation: Mechanism and Process in Physiological Evolution. Oxford Univ. Press, Oxford

Holland H. D., 2002, Geochim. Cosmochim. Acta, 66, 3811

Hu Y., Yang J., 2014, Proc. Natl. Acad. Sci., 111, 629

Huang S.-S., 1959, Am. Sci., 47, 397

Iizuka T., Komiya T., Rino S., Maruyama S., Hirata T., 2010, Geochim. Cosmochim. Acta, 74, 2450

Jin S., Mordasini C., 2018, ApJ, 853, 163

Johnson B. W., Wing B. A., 2020, Nat. Geosci., 13, 243

Judson O. P., 2017, Nat. Ecol. Evol., 1, 0138

Kaltenegger L., 2017, ARA&A, 55, 433

Kaltenegger L., 2019, AAS/Division for Extreme Solar Systems Abstracts, Vol. 51, p. 502.05

Kaltenegger L., Sasselov D., Rugheimer S., 2013, ApJ, 775, L47

Kane S. R. et al., 2019, J. Geophys. Res. Planets, 124, 2015

Kasting J., 2012, How to Find a Habitable Planet. Princeton Univ. Press, Princeton

Kasting J. F., Whitmire D. P., Reynolds R. T., 1993, Icarus, 101, 108

Kasting J. F., Chen H., Kopparapu R. K., 2015, ApJ, 813, L3

Kiang N. Y. et al., 2007, Astrobiology, 7, 252

Kingsolver J. G., 2009, Am. Nat., 174, 755

Kipp M. A., Stüeken E. E., 2017, Sci. Adv., 3, eaao4795

Kirchman D. L., 2018, Processes in Microbial Ecology, 2nd edn. Oxford Univ. Press, Oxford

Kirk J. T. O., 2011, Light and Photosynthesis in Aquatic Ecosystems, 3rd edn. Cambridge Univ. Press, Cambridge

Kite E. S., Ford E. B., 2018, ApJ, 864, 75

Kleinböhl A., Willacy K., Friedson A. J., Chen P., Swain M. R., 2018, ApJ, 862, 92

Knoll A. H., 1985, in Papagiannis M. D., ed., Proc. IAU Symp. 112, The Search for Extraterrestrial Life: Recent Developments. Kluwer, Dordrecht, p. 201

Knoll A. H., 2015, Life on a Young Planet: The First Three Billion Years of Evolution on Earth, Princeton Science Library. Princeton Univ. Press, Princeton

Knoll A. H., Nowak M. A., 2017, Sci. Adv., 3, e1603076

Konhauser K. O., 2007, Introduction to Geomicrobiology. Blackwell Publishing, Oxford

Kopparapu R. K. et al., 2013, ApJ, 765, 131

Kopparapu R. K., Ramirez R. M., SchottelKotte J., Kasting J. F., Domagal-Goldman S., Eymet V., 2014, ApJ, 787, L29

Kopparapu R. K., Wolf E. T., Haqq-Misra J., Yang J., Kasting J. F., Meadows V., Terrien R., Mahadevan S., 2016, ApJ, 819, 84

Kou L., Labrie D., Chylek P., 1993, Appl. Opt., 32, 3531

Kuchner M. J., 2003, ApJ, 596, L105

Kume A., 2019, Color of Photosynthetic Systems: Importance of Atmospheric Spectral Segregation Between Direct and Diffuse Radiation. Springer, Singapore

Laakso T. A., Schrag D. P., 2018, Global Biogeochem. Cy., 32, 486

Laakso T. A., Sperling E. A., Johnston D. T., Knoll A. H., 2020, Proc. Natl. Acad. Sci., 117, 11961

Lane N., 2002, Oxygen: The Molecule that Made the World. Oxford Univ. Press, Oxford

Langford V. S., McKinley A. J., Quickenden T. I., 2001, J. Phys. Chem. A, 105, 8916

Laufkötter C. et al., 2015, Biogeosciences, 12, 6955

Leconte J., Forget F., Charnay B., Wordsworth R., Pottier A., 2013, Nature, 504, 268

Lee Z., Weidemann A., Kindle J., Arnone R., Carder K. L., Davis C., 2007, J. Geophys. Res. Oceans, 112, C03009

Lee Z., Wei J., Voss K., Lewis M., Bricaud A., Huot Y., 2015, Appl. Opt., 54, 546

Lee Z.-P., Darecki M., Carder K. L., Davis C. O., Stramski D., Rhea W. J., 2005, J. Geophys. Res. Oceans, 110, C02017

Léger A. et al., 2004, Icarus, 169, 499

Lehmer O. R., Catling D. C., Parenteau M. N., Hoehler T. M., 2018, ApJ, 859, 171

Lenton T. M., 2020, Interface Focus, 10, 20200018

Lewandowska A. M., Boyce D. G., Hofmann M., Matthiessen B., Sommer U., Worm B., 2014, Ecol. Lett., 17, 614

Leys S. P., Kahn A. S., 2018, Integr. Comp. Biol., 58, 666

Lingam M., 2020, Astron. J., 159, 144

Lingam M., Loeb A., 2017, ApJ, 848, 41

Lingam M., Loeb A., 2018a, Astrobiology, 18, 967

Lingam M., Loeb A., 2018b, Astron. J., 156, 151

Lingam M., Loeb A., 2018c, ApJ, 857, L17

Lingam M., Loeb A., 2019a, Int. J. Astrobiol., 18, 112

Lingam M., Loeb A., 2019b, Rev. Mod. Phys., 91, 021002

Lingam M., Loeb A., 2019c, Astron. J., 157, 25

Lingam M., Loeb A., 2019d, MNRAS, 485, 5924

Lingam M., Loeb A., 2019e, ApJ, 883, 143

Lingam M., Loeb A., 2020a, Int. J. Astrobiol., 19, 210

Lingam M., Loeb A., 2020b, ApJ, 889, L15

Lingam M., Loeb A., 2020c, ApJ, 901, L11

Lingam M., Loeb A., 2021, Life in the Cosmos: From Biosignatures to Technosignatures. Harvard Univ. Press, Cambridge

Lingam M., Ginsburg I., Loeb A., 2020, ApJ, 888, 102

Litjens R. A., Quickenden T. I., Freeman C. G., 1999, Appl. Opt., 38, 1216

Luger R., Barnes R., 2015, Astrobiology, 15, 119

Lunine J. I., 2013, Earth: Evolution of a Habitable World, 2nd edn. Cambridge Univ. Press, Cambridge

McKay C. P., 1996, Circumstellar Habitable Zones. Travis House Publications, Menlo Park

McKay C. P., 2014, Proc. Natl. Acad. Sci., 111, 12628

McMahon S., Parnell J., 2014, FEMS Microbiol. Ecol., 87, 113

McMahon S., O'Malley-James J., Parnell J., 2013, Planet. Space Sci., 85, 312

Madhusudhan N., 2019, ARA&A, 57, 617

Mann K. H., Lazier J. R. N., 2006, Dynamics of Marine Ecosystems: Biological-Physical Interactions in the Oceans, 3rd edn. Blackwell Publishing, Oxford

Marañón E., Lorenzo M. P., Cermeño P., Mouriño-Carballido B., 2018, ISME J., 12, 1836

Marra J., 2004, Geophys. Res. Lett., 31, L06305

Marra J. F., Lance V. P., Vaillancourt R. D., Hargreaves B. R., 2014, Deep-Sea Res., 83, 45

Marshall S. M., Orr A. P., 1928, J. Mar. Biol. Ass., 15, 321

Martins Z. et al., 2017, Space Sci. Rev., 209, 43

Meadows V. S. et al., 2018, Astrobiology, 18, 630

Merino N., Aronson H. S., Bojanova D. P., Feyhl-Buska J., Wong M. L., Zhang S., Giovannelli D., 2019, Frontier Microbiol., 10, 780

Middelburg J. J., 2019, Marine Carbon Biogeochemistry: A Primer for Earth System Scientists, SpringerBriefs in Earth System Sciences. Springer, Cham

Mills E. L., 2012, Biological Oceanography: An Early History, 1870-1960. University of Toronto Press, Canada

Mills D. B., Ward L. M., Jones C., Sweeten B., Forth M., Treusch A. H., Canfield D. E., 2014, Proc. Natl. Acad. Sci., 111, 4168

Morel A., Maritorena S., 2001, J. Geophys. Res., 106, 7163

Morel A., Gentili B., Claustre H., Babin M., Bricaud A., Ras J., Tièche F., 2007, Limnol. Oceanogr., 52, 217

Mundim K. C., Baraldi S., Machado H. G., Vieira F. M. C., 2020, Ecol. Model., 431, 109127

Murante G. et al., 2020, MNRAS, 492, 2638

Nelson D. M., Smith W. O., 1991, Limnol. Oceanogr., 36, 1650

Noack L., Snellen I., Rauer H., 2017, Space Sci. Rev., 212, 877

Nürnberg D. J. et al., 2018, Science, 360, 1210

O'Malley-James J. T., Kaltenegger L., 2019, ApJ, 879, L20

O'Malley-James J. T., Greaves J. S., Raven J. A., Cockell C. S., 2013, Int. J. Astrobiol., 12, 99

O'Malley-James J. T., Cockell C. S., Greaves J. S., Raven J. A., 2014, Int. J. Astrobiol., 13, 229

Obata A., Ishizaka J., Endoh M., 1996, J. Geophys. Res., 101, 20

Olson S. L., Jansen M., Abbot D. S., 2020, ApJ, 895, 19

Orcutt B. N., Sylvan J. B., Knab N. J., Edwards K. J., 2011, Microbiol. Mol. Biol. Rev., 75, 361

Padfield D., Yvon-Durocher G., Buckling A., Jennings S., Yvon-Durocher G., 2016, Ecol. Lett., 19, 133

Pasek M., Omran A., Lang C., Gull M., Abbatiello J., Feng T., Garong L., Abbott-Lyon H., 2020, Serpentinization as a Route to Liberating Phosphorus on Habitable Worlds, Available at: https://www.researchsquare.com/article/rs-37651/v1

Pawlowicz R., 2013, Nat. Educ. Knowl., 4, 13

Pope R. M., Fry E. S., 1997, Appl. Opt., 36, 8710

Popp M., Schmidt H., Marotzke J., 2016, Nat. Commun., 7, 10627

Ramirez R. M., 2018, Geosciences, 8, 280

Ramirez R. M., 2020, Sci. Rep., 10, 7432

Ramirez R. M., Levi A., 2018, MNRAS, 477, 4627

Ramirez R. et al., 2019, BAAS, 51, 31

Raven J. A., 2009, Aquat. Microb. Ecol., 56, 177

Regaudie-De-Gioux A., Duarte C. M., 2010, Global Biogeochem. Cy., 24, GB4013

Regaudie-De-Gioux A., Duarte C. M., 2012, Global Biogeochem. Cy., 26, GB1015

Reinhard C. T., Planavsky N. J., Olson S. L., Lyons T. W., Erwin D. H., 2016, Proc. Natl. Acad. Sci., 113, 8933

Reinhard C. T., Olson S. L., Schwieterman E. W., Lyons T. W., 2017, Astrobiology, 17, 287

Riley G. A., 1946, J. Mar. Res., 6, 54

Ritchie R. J., Larkum A. W. D., Ribas I., 2018, Int. J. Astrobiol., 17, 147

Rogers L. A., 2015, ApJ, 801, 41

Rothschild L. J., Mancinelli R. L., 2001, Nature, 409, 1092

Röttgers R., McKee D., Utschig C., 2014, Opt. Express, 22, 25093

Rushby A. J., Claire M. W., Osborn H., Watson A. J., 2013, Astrobiology, 13, 833

Salazar A. M., Olson S. L., Komacek T. D., Stephens H., Abbot D. S., 2020, ApJ, 896, L16

Sarmiento J. L., Gruber N., 2006, Ocean Biogeochemical Dynamics. Princeton Univ. Press, Princeton

Sathyendranath S., Ji R., Browman H. I., 2015, ICES J. Mar. Sci., 72, 1892

Saulquin B., Hamdi A., Gohin F., Populus J., Mangin A., d'Andon O. F., 2013, Remote Sens. Environ., 128, 224

Scalo J. et al., 2007, Astrobiology, 7, 85

Schaum C.-E. et al., 2017, Nat. Ecol. Evol., 1, 0094

Schlesinger W. H., Bernhardt E. S., 2013, Biogeochemistry: An Analysis of Global Change, 3rd edn. Academic Press, Amsterdam

Schoolfield R. M., Sharpe P. J. H., Magnuson C. E., 1981, J. Theor. Biol., 88, 719

Schulte P. M., 2015, J. Exp. Biol., 218, 1856

Schwieterman E. W. et al., 2018, Astrobiology, 18, 663

Schwieterman E. W., Reinhard C. T., Olson S. L., Harman C. E., Lyons T. W., 2019, ApJ, 878, 19

Seager S., Turner E. L., Schafer J., Ford E. B., 2005, Astrobiology, 5, 372

Sharpe P. J. H., DeMichele D. W., 1977, J. Theor. Biol., 64, 649

Shields A. L., Ballard S., Johnson J. A., 2016, Phys. Rep., 663, 1

Siegel D. A., Doney S. C., Yoder J. A., 2002, Science, 296, 730

Silva L., Vladilo G., Schulte P. M., Murante G., Provenzale A., 2017, Int. J. Astrobiol., 16, 244

Sinclair B. J. et al., 2016, Ecol. Lett., 19, 1372

Smetacek V., Passow U., 1990, Limnol. Oceanogr., 35, 228

Smith R. C., Baker K. S., 1981, Appl. Opt., 20, 177

Son S., Wang M., 2015, Remote Sens. Environ., 159, 250

Sperling E. A., Knoll A. H., Girguis P. R., 2015, Annu. Rev. Ecol. Evol. Syst., 46, 215

Stüeken E. E. et al., 2020, Space Sci. Rev., 216, 31

Sullivan J. M., Twardowski M. S., Zaneveld J. R. V., Moore C. M., Barnard A. H., Donaghay P. L., Rhoades B., 2006, Appl. Opt., 45, 5294

Sverdrup H. U., 1953, J. Cons. Perm. Int. Explor. Mer., 18, 287

Sverdrup H. U., Johnson M. W., Fleming R. H., 1942, The Oceans: Their Physics, Chemistry, and General Biology. Prentice-Hall, New York

Syverson D. D. et al., 2020, preprint (arXiv:2002.07667)

Takizawa K., Minagawa J., Tamura M., Kusakabe N., Narita N., 2017, Sci. Rep., 7, 7561

Tarter J. C. et al., 2007, Astrobiology, 7, 30

Taucher J., Oschlies A., 2011, Geophys. Res. Lett., 38, L02603

Thomas M. K., Aranguren-Gassis M., Kremer C. T., Gould M. R., Anderson K., Klausmeier C. A., Litchman E., 2017, Glob. Change Biol., 23, 3269

Tinetti G., Rashby S., Yung Y. L., 2006, ApJ, 644, L129

Tyrrell T., 1999, Nature, 400, 525

Uitz J., Claustre H., Gentili B., Stramski D., 2010, Global Biogeochem. Cy., 24, GB3016

Unterborn C. T., Hinkel N. R., Desch S. J., 2018, Res. Notes AAS, 2, 116

Valiela I., 2015, Marine Ecological Processes, 3rd edn. Springer-Verlag, New York

Ward L. M., Rasmussen B., Fischer W. W., 2019, J. Geophys. Res. Biogeosci., 124, 211

Westberry T., Behrenfeld M. J., Siegel D. A., Boss E., 2008, Global Biogeochem. Cy., 22, GB2024

Wheat C. G., Feely R. A., Mottl M. J., 1996, Geochim. Cosmochim. Acta, 60, 3593

Willmer P., Stone G., Johnston I., 2005, Environmental Physiology of Animals, 2nd edn. Blackwell Publishing, Malden

Wolf E. T., Toon O. B., 2015, J. Geophys. Res. D, 120, 5775

Wolf E. T., Shields A. L., Kopparapu R. K., Haqq-Misra J., Toon O. B., 2017, ApJ, 837, 107

Wolfgang A., Lopez E., 2015, ApJ, 806, 183
Wolstencroft R. D., Raven J. A., 2002, Icarus, 157, 535
Wordsworth R. D., Pierrehumbert R. T., 2013, ApJ, 778, 154
Wordsworth R., Pierrehumbert R., 2014, ApJ, 785, L20
Yamashiki Y. A. et al., 2019, ApJ, 881, 114
Yang J., Cowan N. B., Abbot D. S., 2013, ApJ, 771, L45
Yang J., Abbot D. S., Koll D. D. B., Hu Y., Showman A. P., 2019, ApJ, 871, 29
Yvon-Durocher G. et al., 2012, Nature, 487, 472

Zeng L., Jacobsen S. B., Sasselov D. D., Vanderburg A., 2018, MNRAS, 479, 5567
Zhang X., Cui L., 2016, J. Earth Sci., 27, 187
Zsom A., Seager S., de Wit J., Stamenković V., 2013, ApJ, 778, 109

This paper has been typeset from a TEX/LATEX file prepared by the author.